Electronic Supporting Information

The effect of ionic versus covalent functionalization of Polyoxometalate hybrid materials with coordinating subunits on their stability and interaction with DNA

Daria Nowicka[#a], Dawid Marcinkowski[#a], Nahir Vadra[b], Martyna Szymańska[a], Maciej Kubicki[a], Giuseppe Consiglio[c], Wojciech Drożdż[ad], Artur R. Stefankiewicz[ad], Violetta Patroniak[a], Marta Fik-Jaskółka*[a] and Adam Gorczyński*[a]

[a] *Adam Mickiewicz University in Poznań, Faculty of Chemistry, Uniwersytetu Poznańskiego 8, 61-614 Poznań, Poland*

[b] *Universidad de Buenos Aires, Facultad de Ciencias Exactas y Naturales, Departamento de Química Inorgánica, Analítica y Química Física and CONICET–Universidad de Buenos Aires, Instituto de Química Física de los Materiales, Medio Ambiente y Energía (INQUIMAE), Buenos Aires C1428EGA, Argentina*

[c] *Università di Catania, Dipartimento di Scienze Chimiche, I-95125 Catania, Italy*

[d] *Adam Mickiewicz University in Poznań, Center for Advanced Technology, Uniwersytetu Poznańskiego 10, 61-614 Poznań, Poland*

** Correspondence: marta.fik@amu.edu.pl; adam.gorczynski@amu.edu.pl*

 # equal contribution†

Table of contents for Electronic Supporting Information

1. Schematic synthesis of ligand, complexes and hybrids

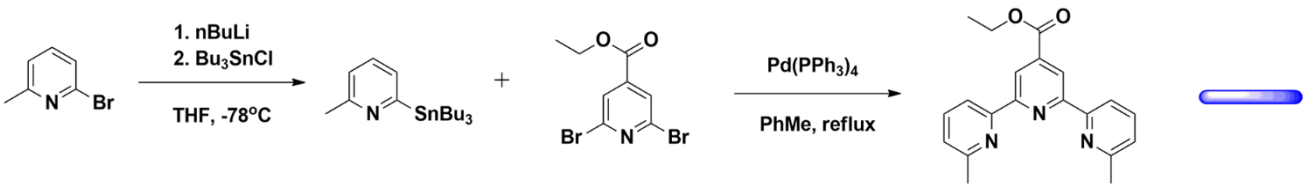

Scheme S1. Scheme of synthesis of ligand $\mathbf{L^{tpy}}$ [$C_{20}H_{19}N_3O_2$] according to publication [1].

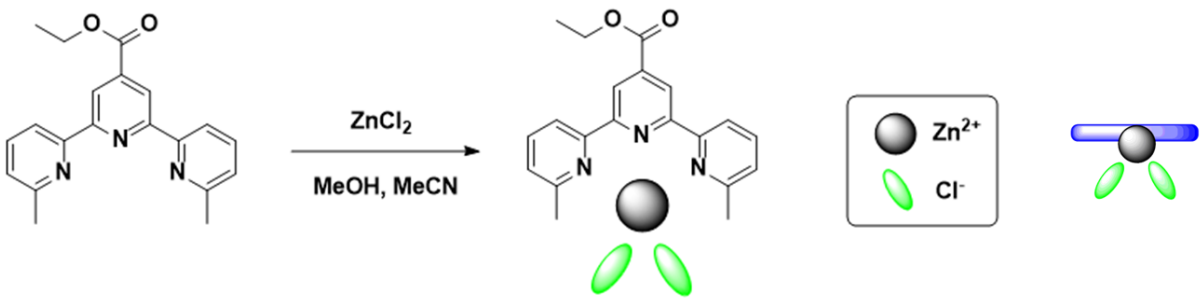

Scheme S2. Scheme of synthesis of complex **K1 [$\mathbf{ZnL^{tpy}Cl_2}$]**.

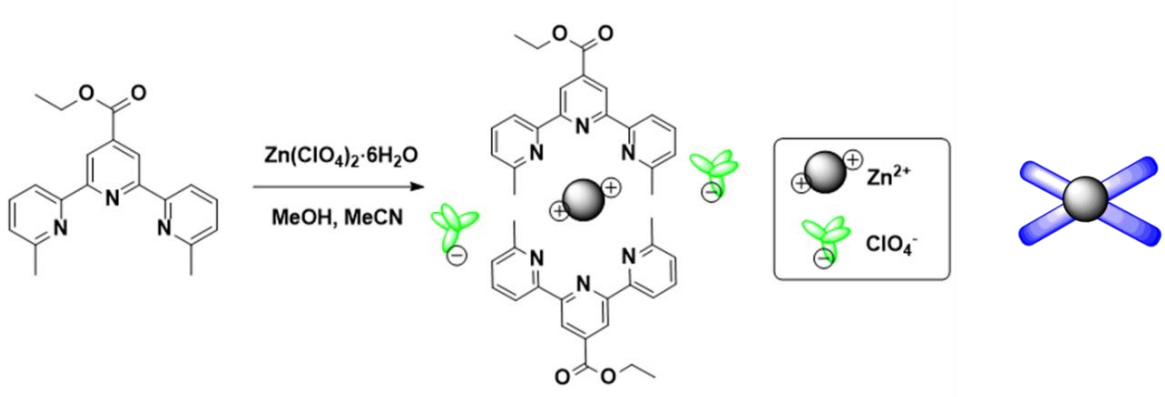

Scheme S3. Scheme of synthesis of complex **K2 [$\mathbf{Zn(L^{tpy})_2](ClO_4)_2}$**.

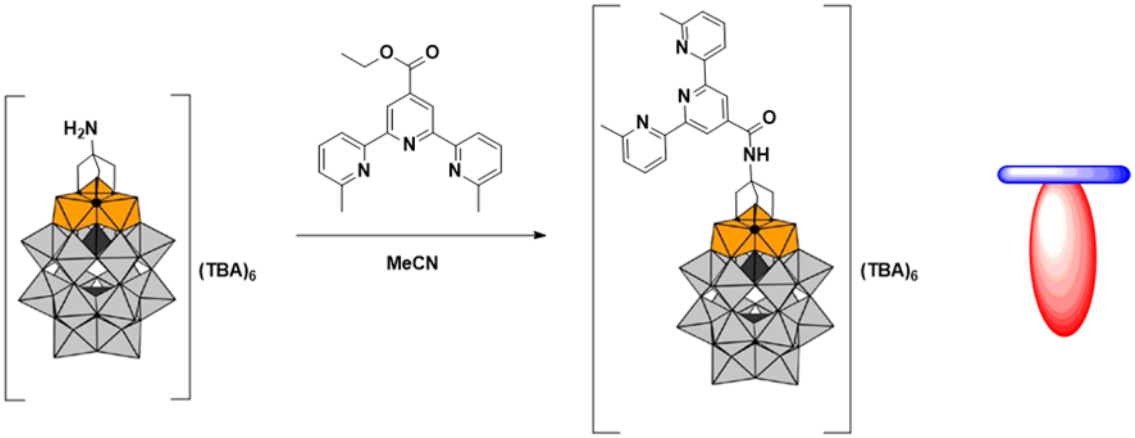

Scheme S4. Scheme of synthesis of hybrid **H1^{cov} (POM + L^{tpy})**.

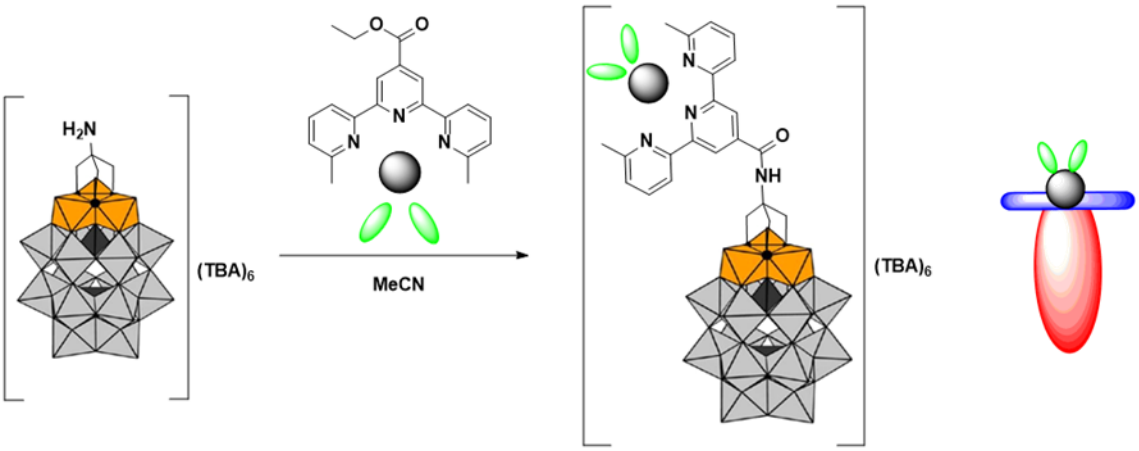

Scheme S5. Scheme of synthesis of hybrid **H2^{cov} (POM + K1)**.

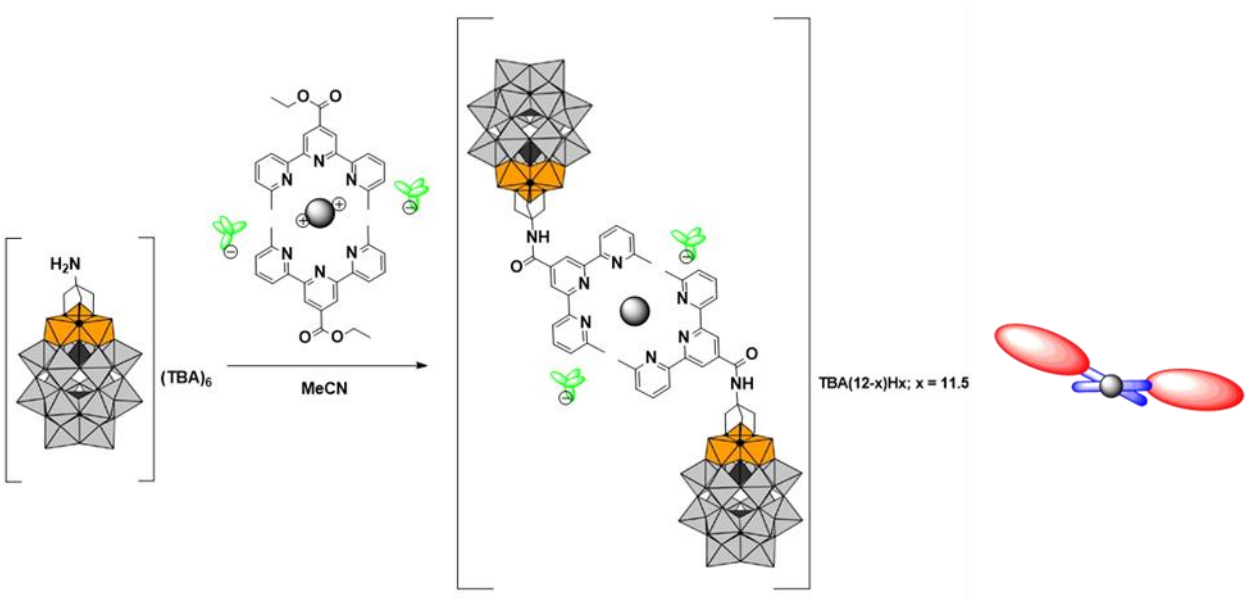

Scheme S6. Scheme of synthesis of hybrid **H3^{cov} (POM + K2)**.

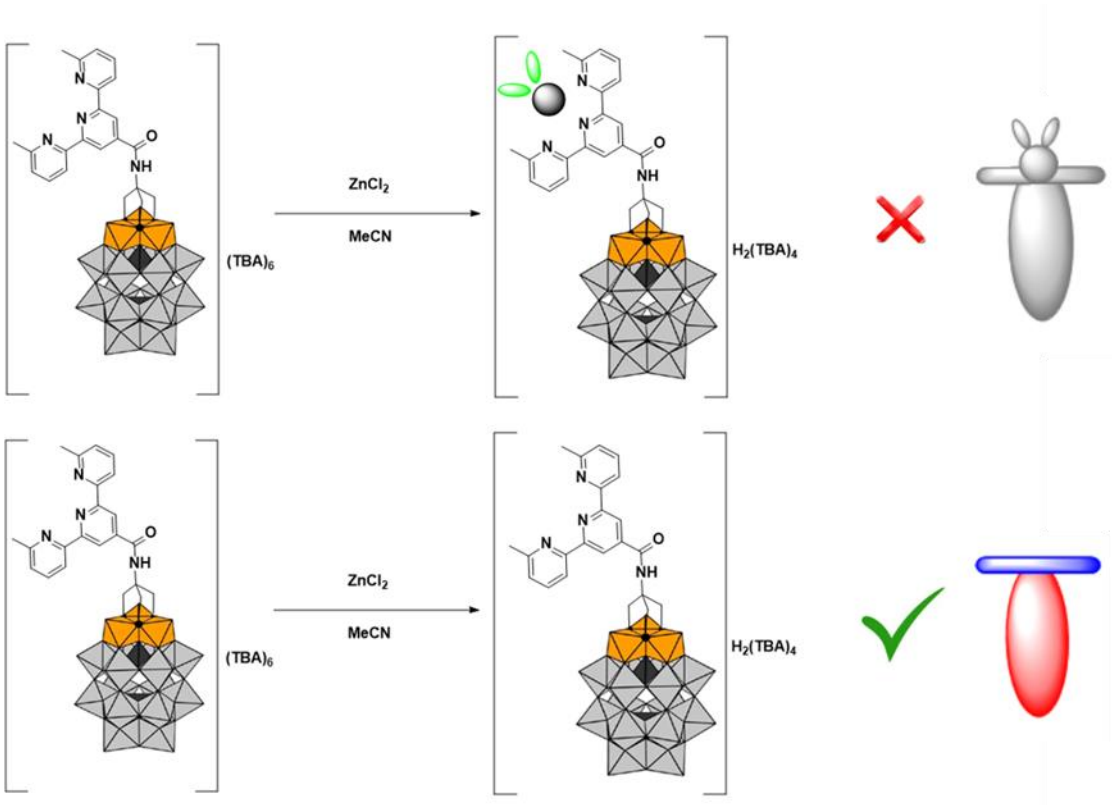

Scheme S7. Scheme of synthesis of hybrid **H4^{cov} (H1^{cov} + $ZnCl_2$)**.

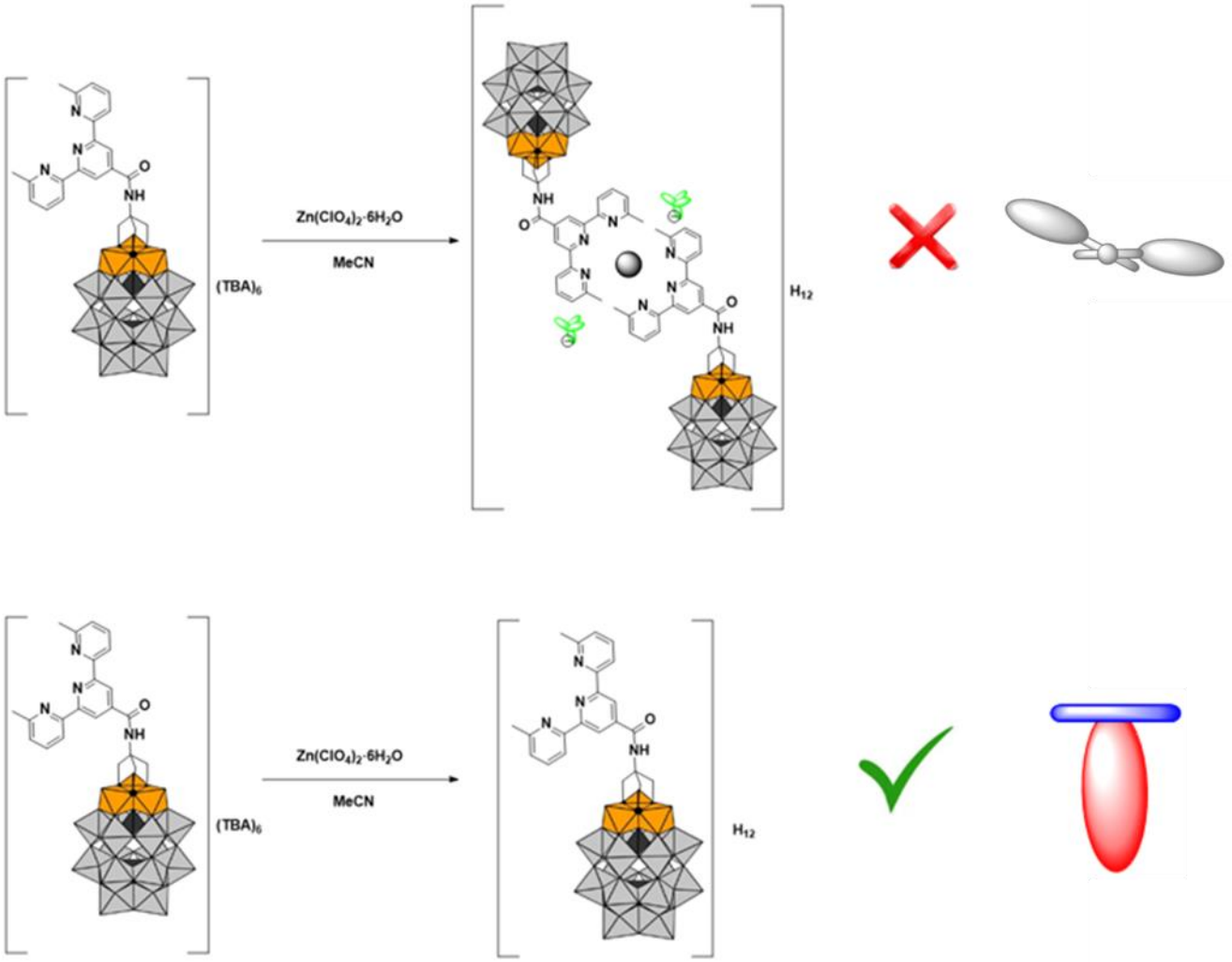

Scheme S8. Scheme of synthesis of hybrid **H5^{cov} (H1^{cov} + Zn(ClO$_4$)$_2$)**.

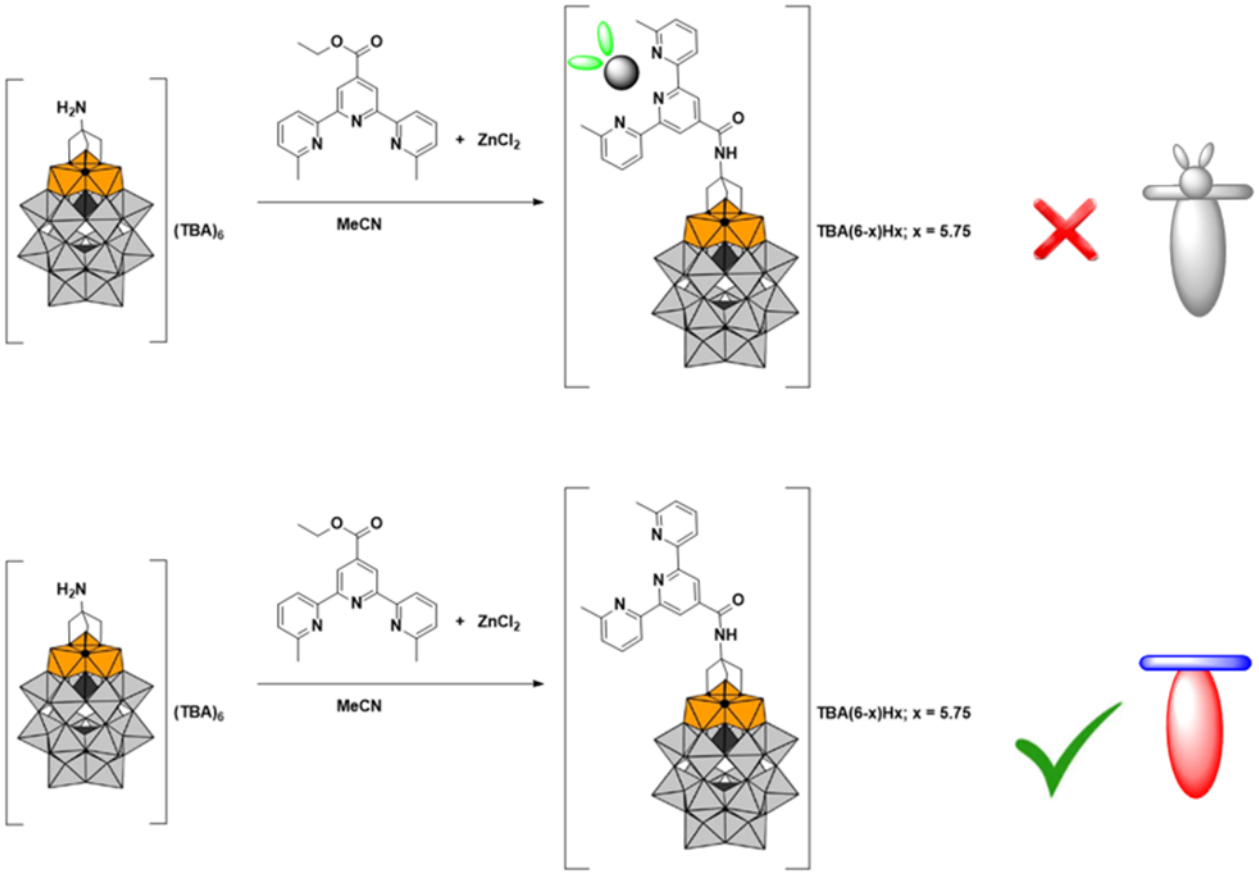

Scheme S9. Scheme of synthesis of hybrid **H6^{cov} (POM + L^{tpy} + ZnCl$_2$)**.

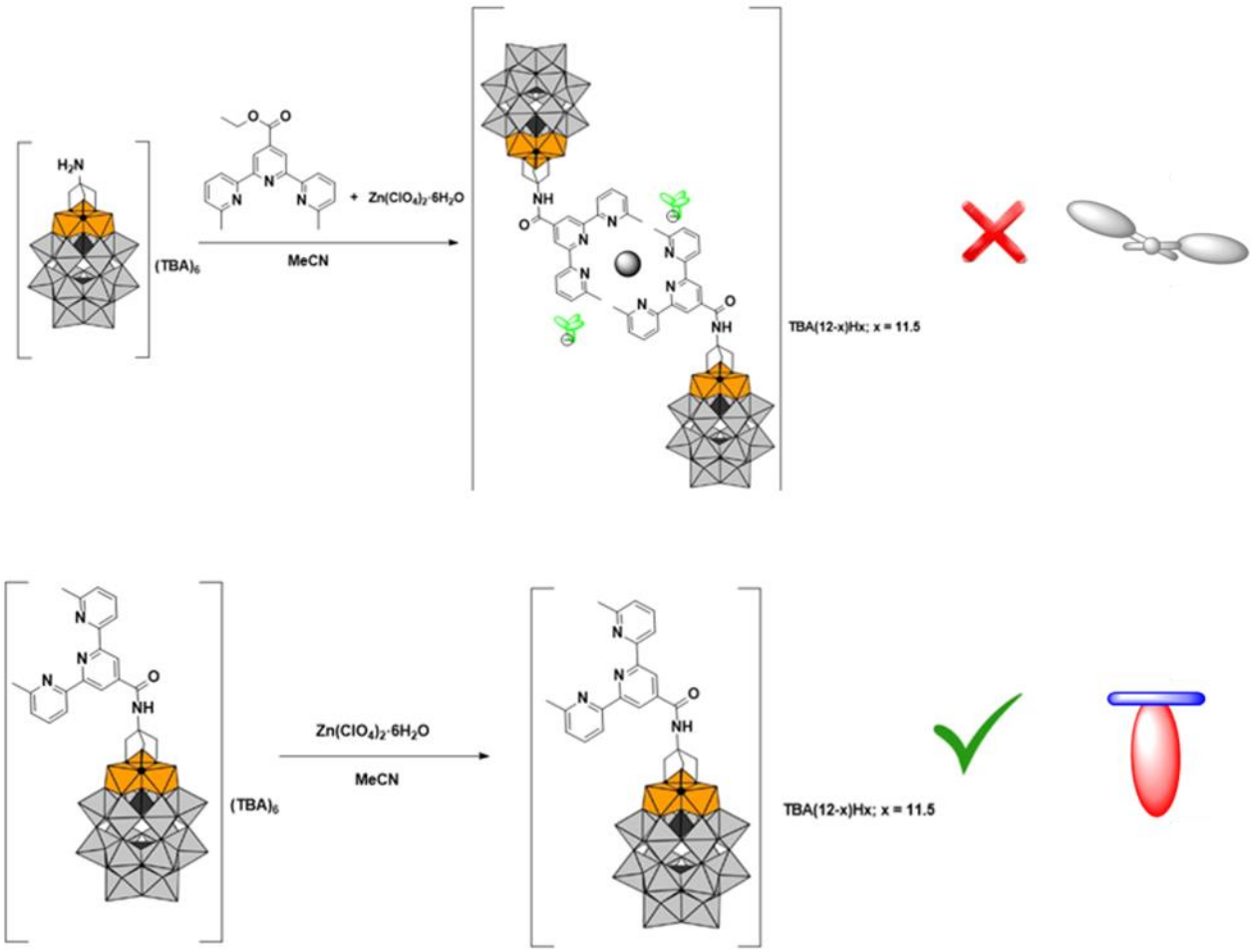

Scheme S10. Scheme of synthesis of hybrid **H7^{cov} (POM + L^{tpy} + Zn(ClO$_4$)$_2$)**.

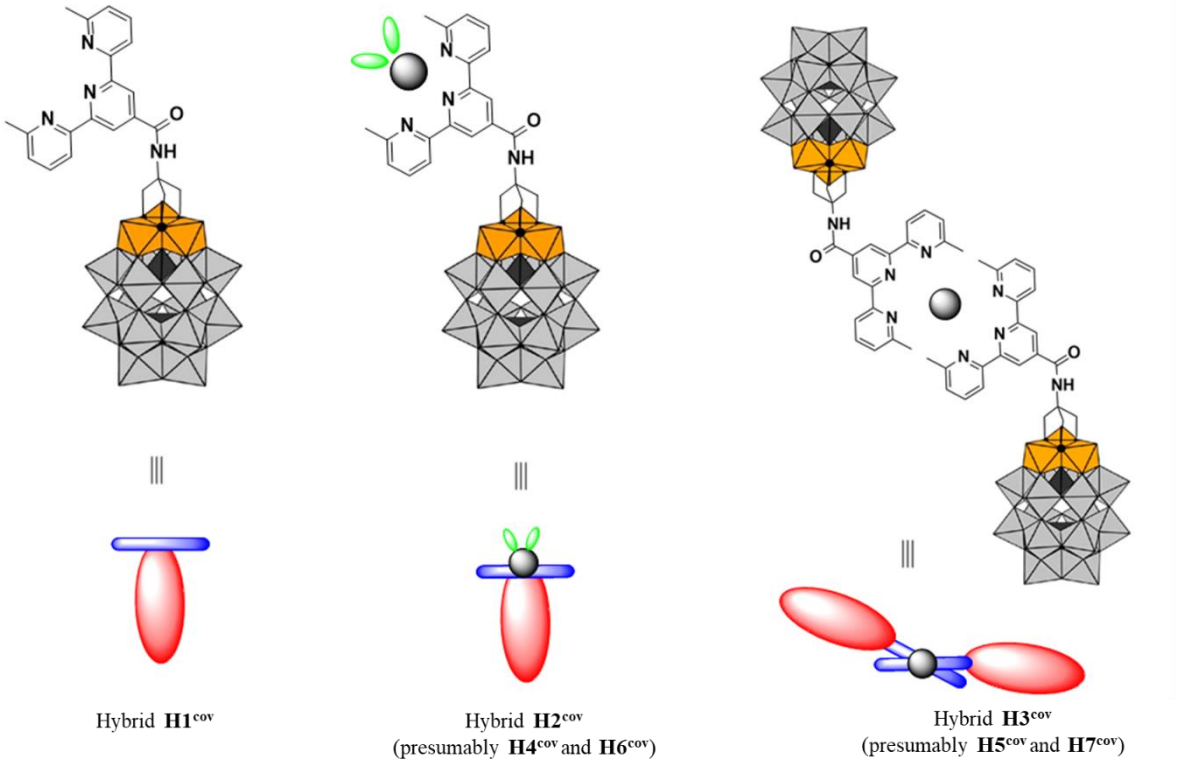

Scheme S11. Schematic representation structures of hybrids **H1^{cov} - H7^{cov}**.

2. FT-IR spectra of ligand, complexes and hybrids

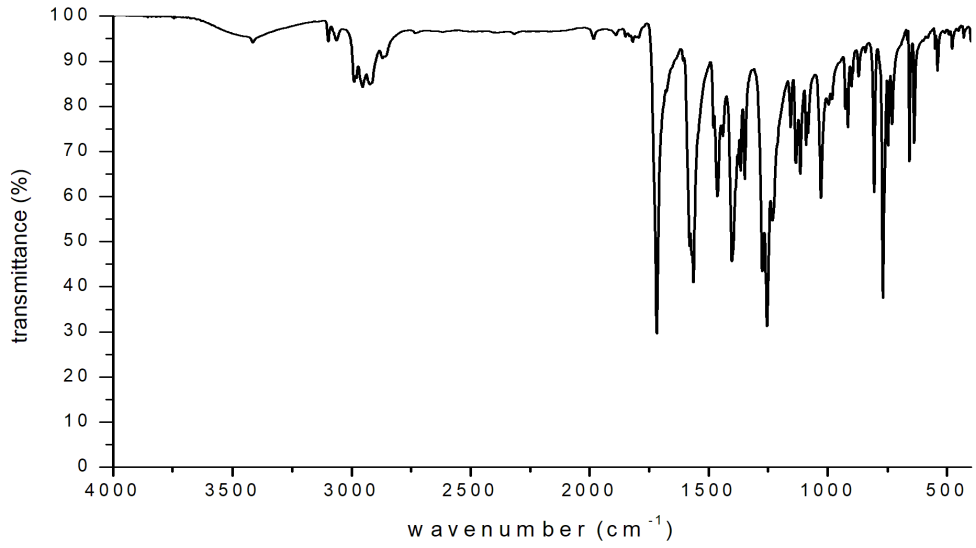

Fig. S1. IR spectrum of ligand **L^{tpy}**.

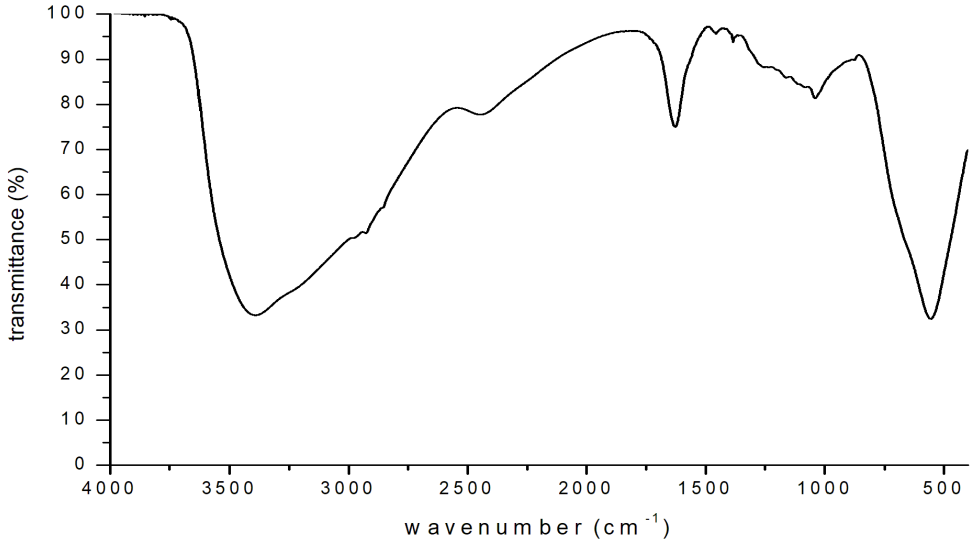

Fig. S2. IR spectrum of complex **K1**.

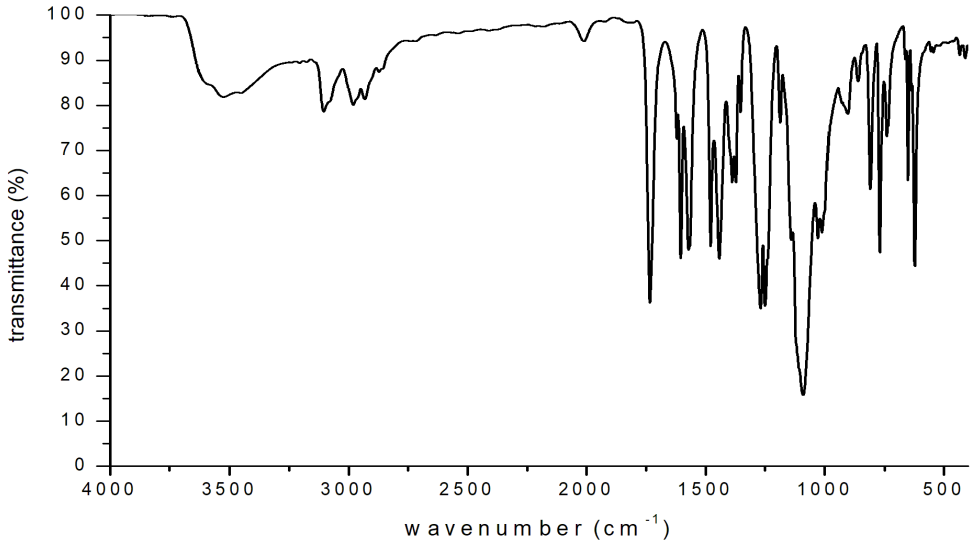

Fig. S3. IR spectrum of complex **K2**.

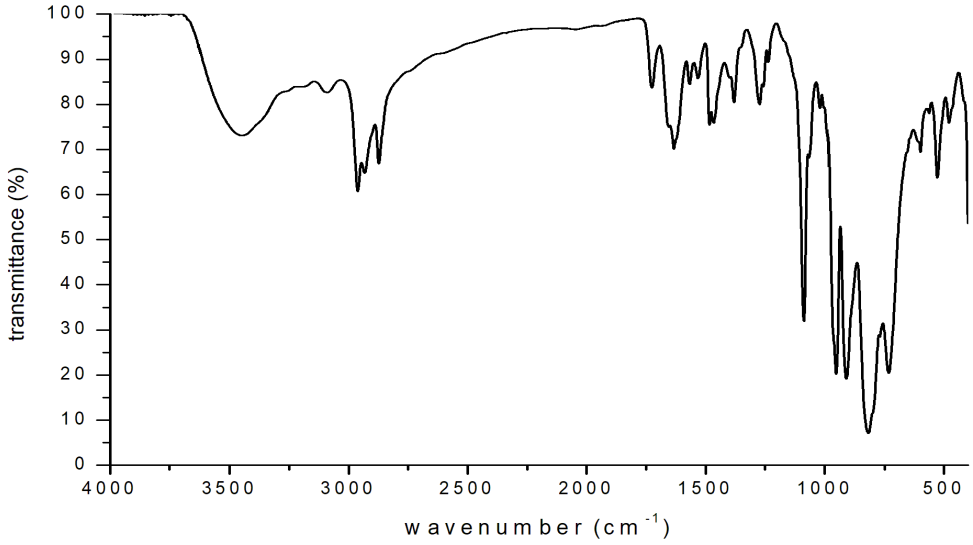

Fig. S4. IR spectrum of hybrid **H1^{cov} (POM + L^{tpy})**.

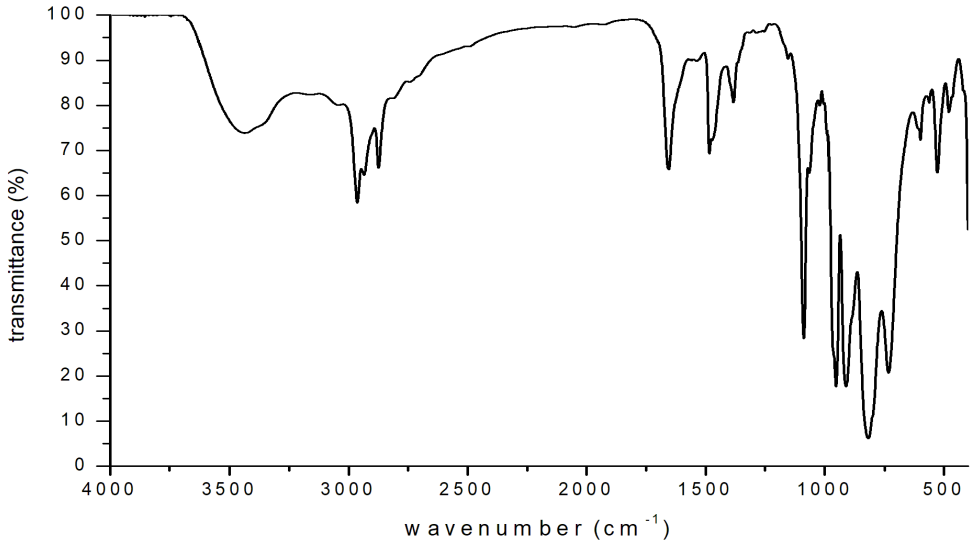

Fig. S5. IR spectrum of hybrid **H2^{cov} (POM + K1)**.

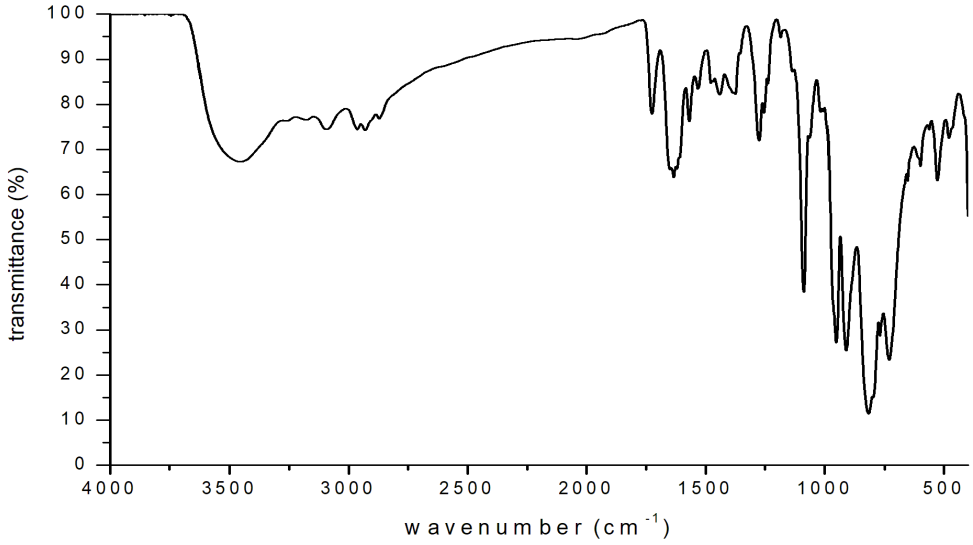

Fig. S6. IR spectrum of hybrid **H3^{cov} (POM + K2)**.

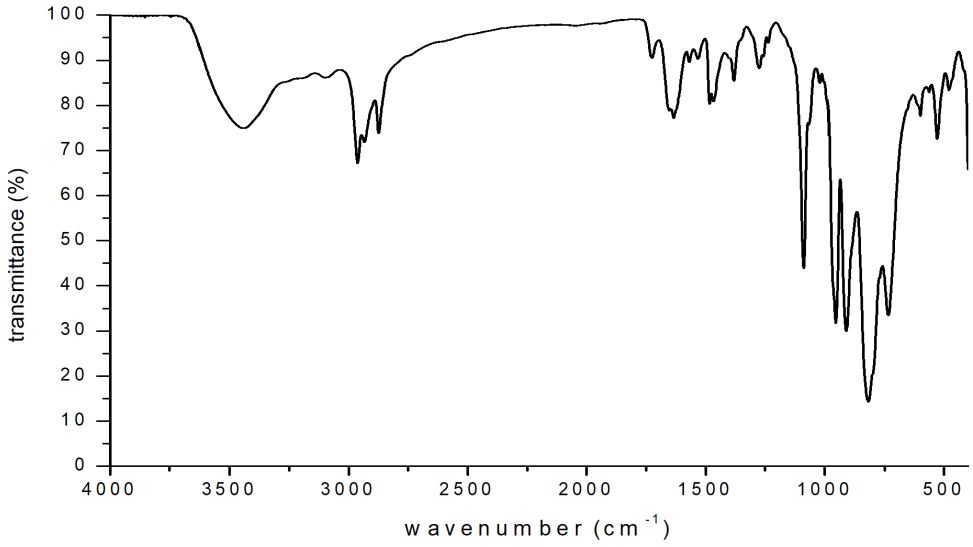

Fig. S7. IR spectrum of hybrid **H4^{cov} (H1^{cov} + $ZnCl_2$)**.

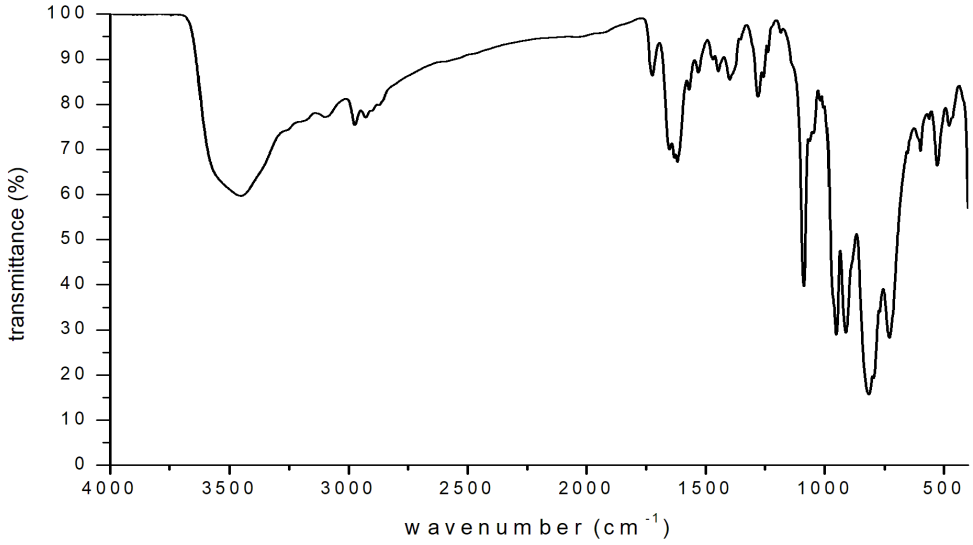

Fig. S8. IR spectrum of hybrid **H5^{cov} (H1^{cov} + Zn(ClO$_4$)$_2$)**.

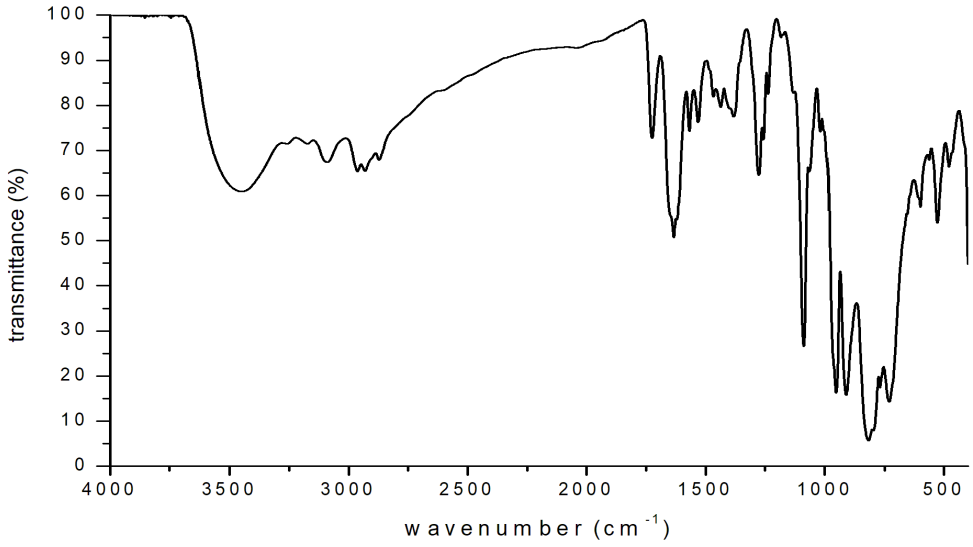

Fig. S9. IR spectrum of hybrid **H6^{cov} (POM + L^{tpy} + ZnCl$_2$)**.

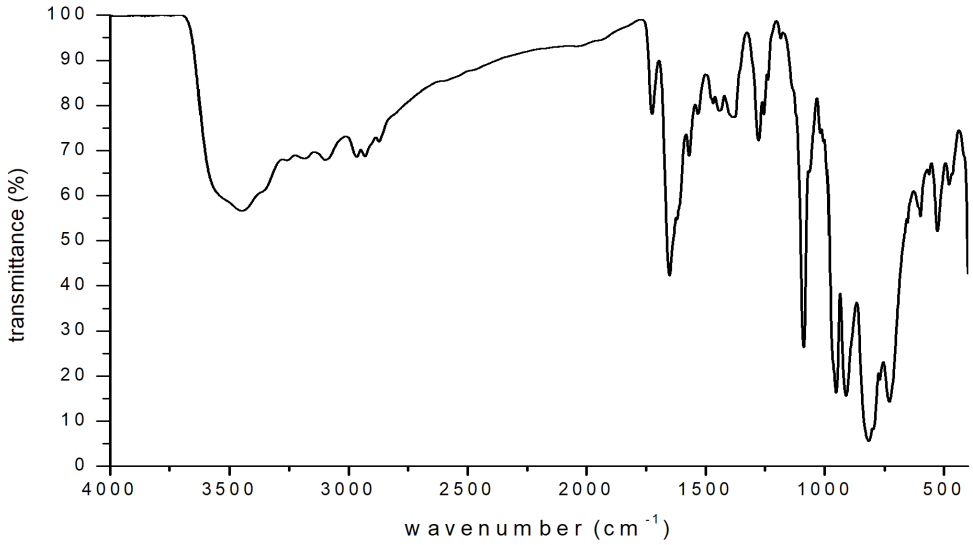

Fig. S10. IR spectrum of hybrid **H7^{cov} (POM + L^{tpy} + Zn(ClO$_4$)$_2$)**.

3. Comparison of IR spectra of compounds

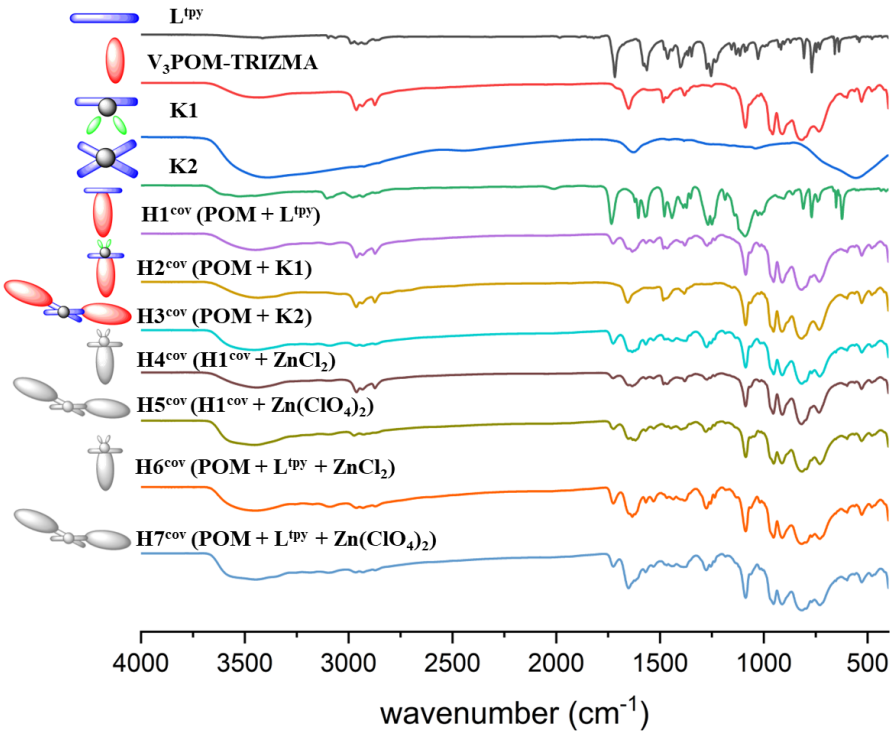

Fig. S11. Comparison of IR spectra of compounds: **L^{tpy}**, **V$_3$POM-TRIZMA**, **K1**, **K2**, **V$_3$POM-TBA, H1^{cov} (POM + L^{tpy}), H2^{cov} (POM + K1), H3^{cov} (POM + K2), H4^{cov} (H1^{cov} + ZnCl$_2$), H5^{cov} (H1^{cov} + Zn(ClO$_4$)$_2$), H6^{cov} (POM + L^{tpy} + ZnCl$_2$), H7^{cov} (POM + L^{tpy} + Zn(ClO$_4$)$_2$)**, respectively.

4. ^{1}H NMR spectra of ligand, complexes and hybrids

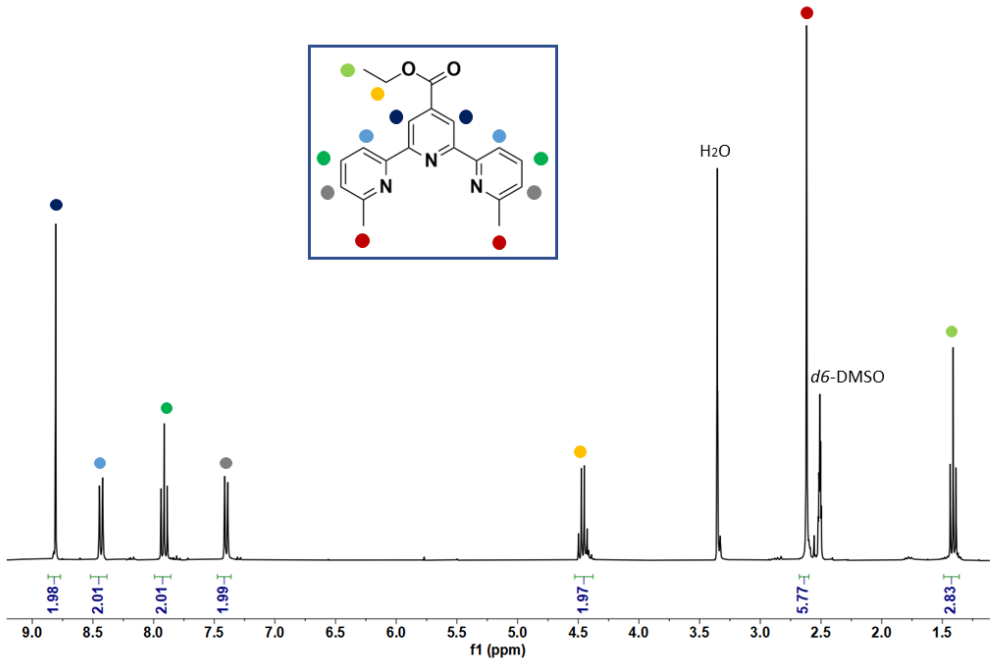

Fig. S12. ^{1}H NMR spectrum of ligand $\mathbf{L^{tpy}}$ in $CDCl_3$ at 400 MHz.

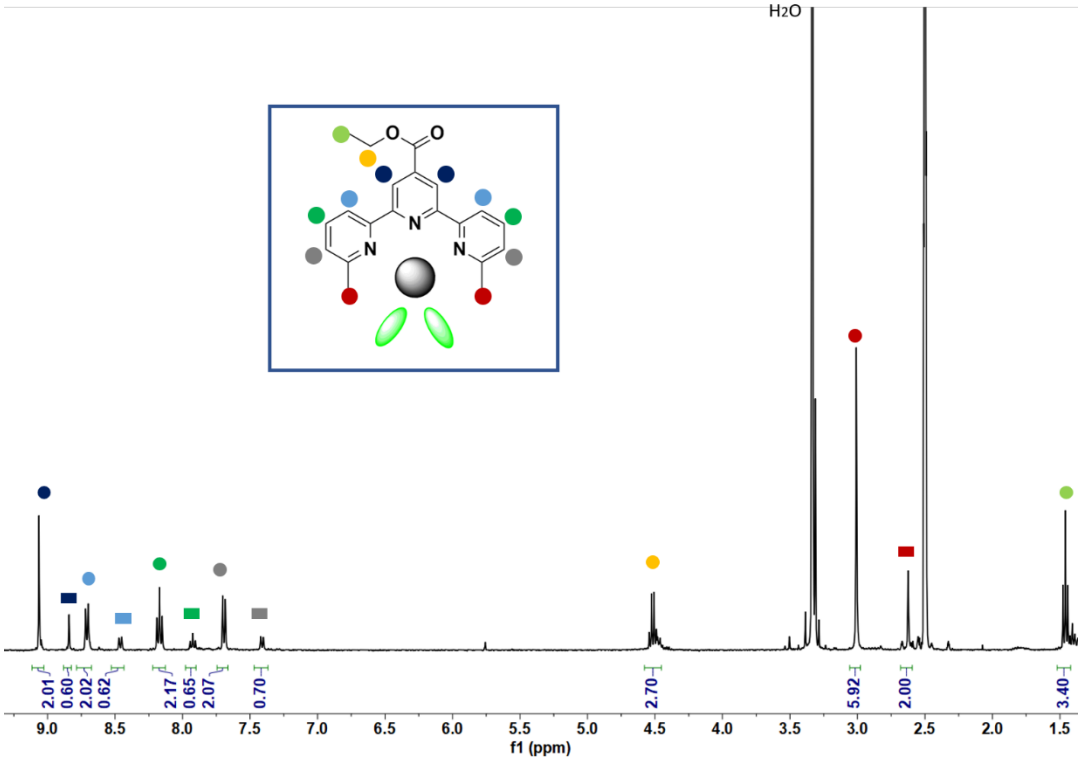

Fig. S13. ^{1}H NMR spectrum of complex **K1** in *d6*-DMSO at 400 MHz.

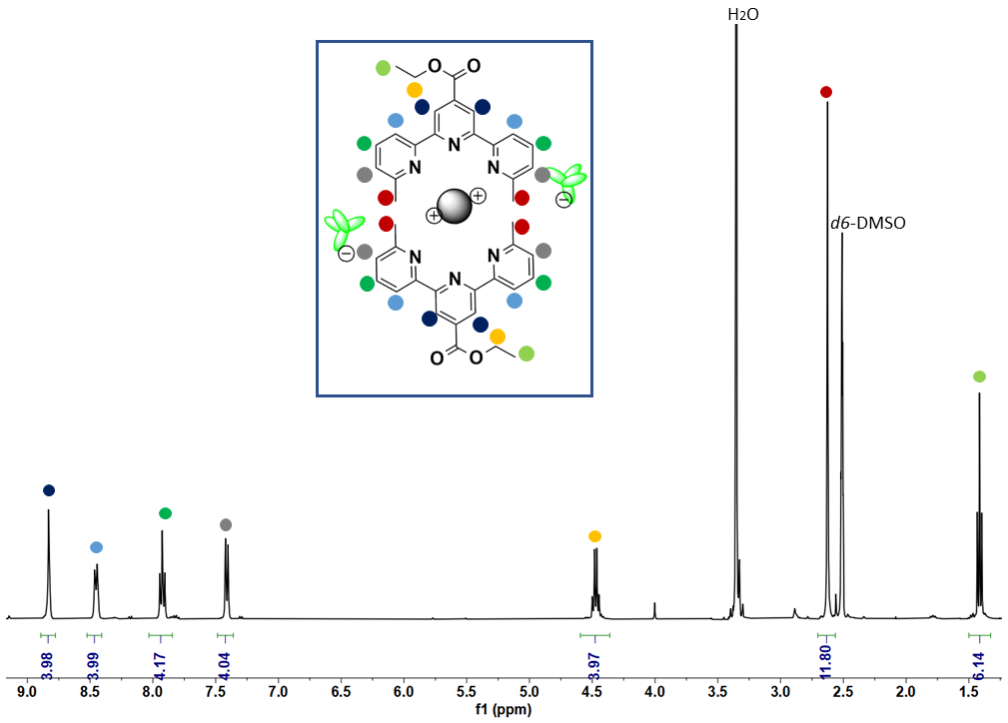

Fig. S14. ^{1}H NMR spectrum of complex **K2** in *d6*-DMSO at 400 MHz.

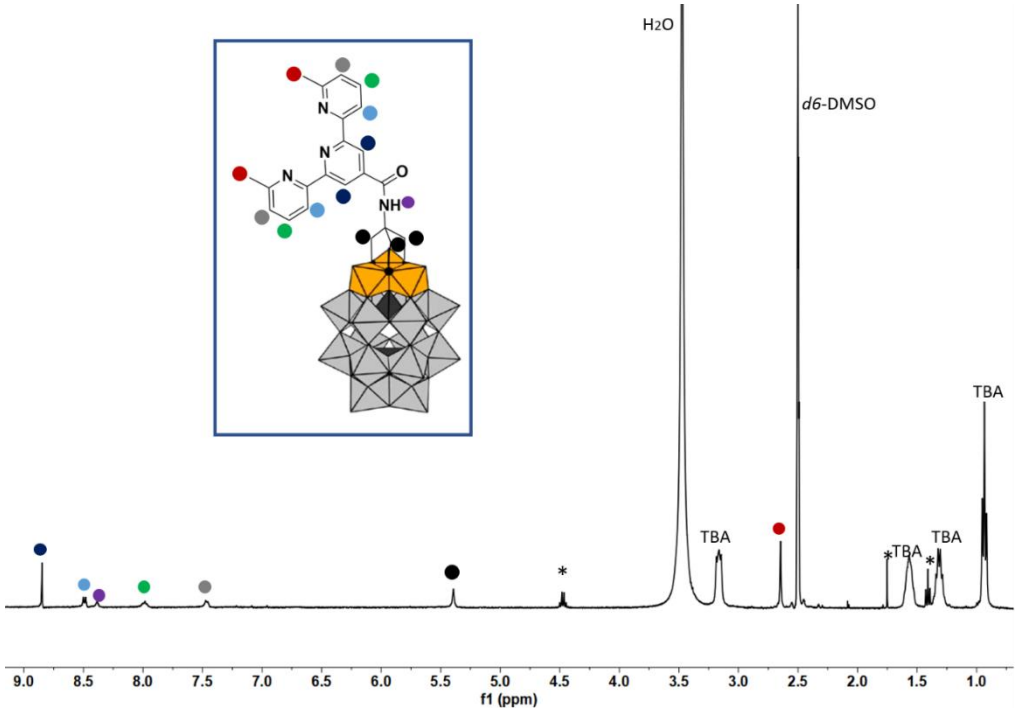

Fig. S15. ^{1}H NMR spectrum of hybrid **H1^{cov} (POM + L^{tpy})** in DMSO-d_6 at 400 MHz.

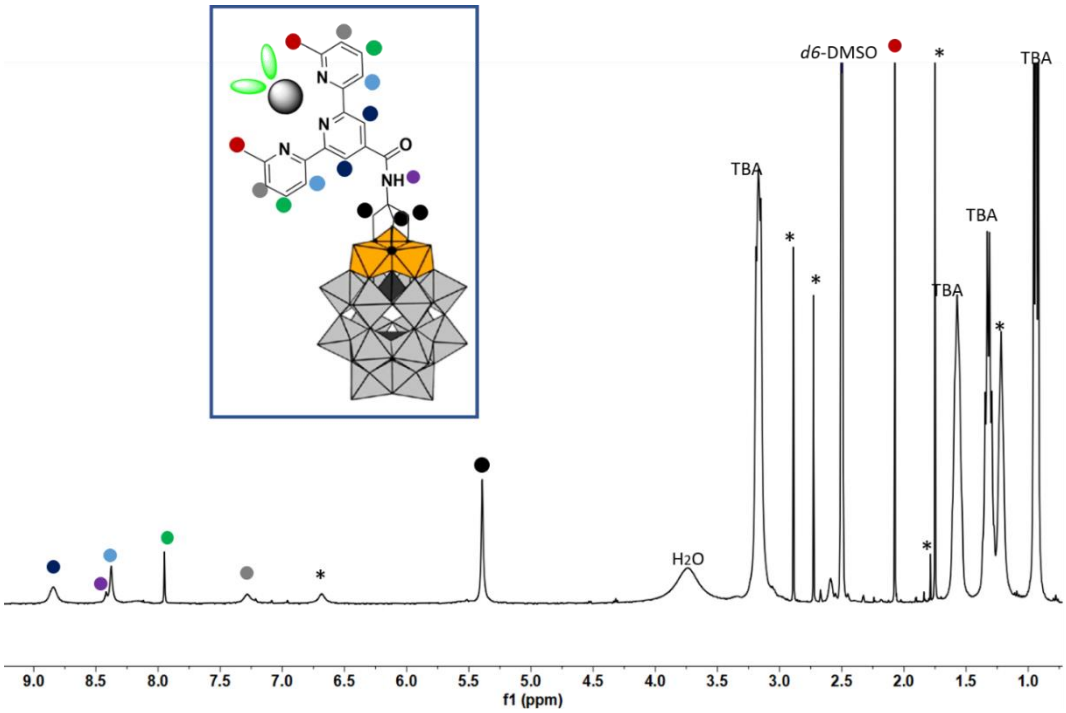

Fig. S16. ^{1}H NMR spectrum of hybrid **H2^{cov} (POM + K1)** in DMSO-d_6 at 400 MHz.

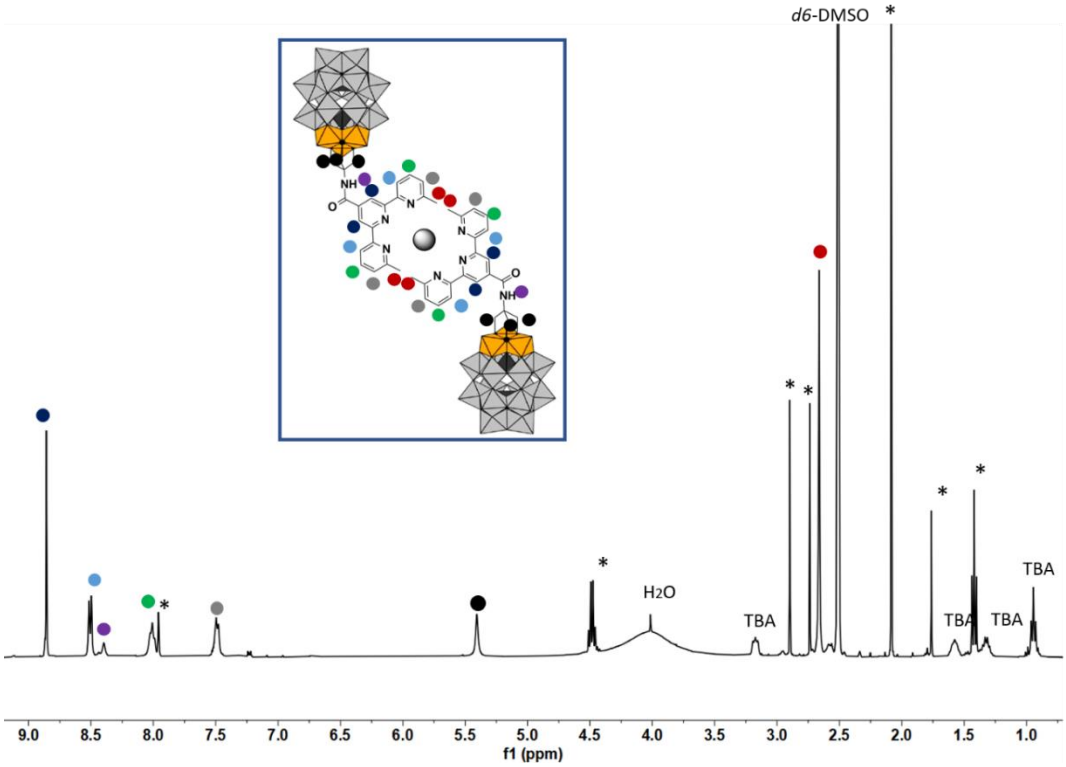

Fig. S17. ^{1}H NMR spectrum of hybrid **H3^{cov} (POM + K2)** in DMSO-d_6 at 400 MHz.

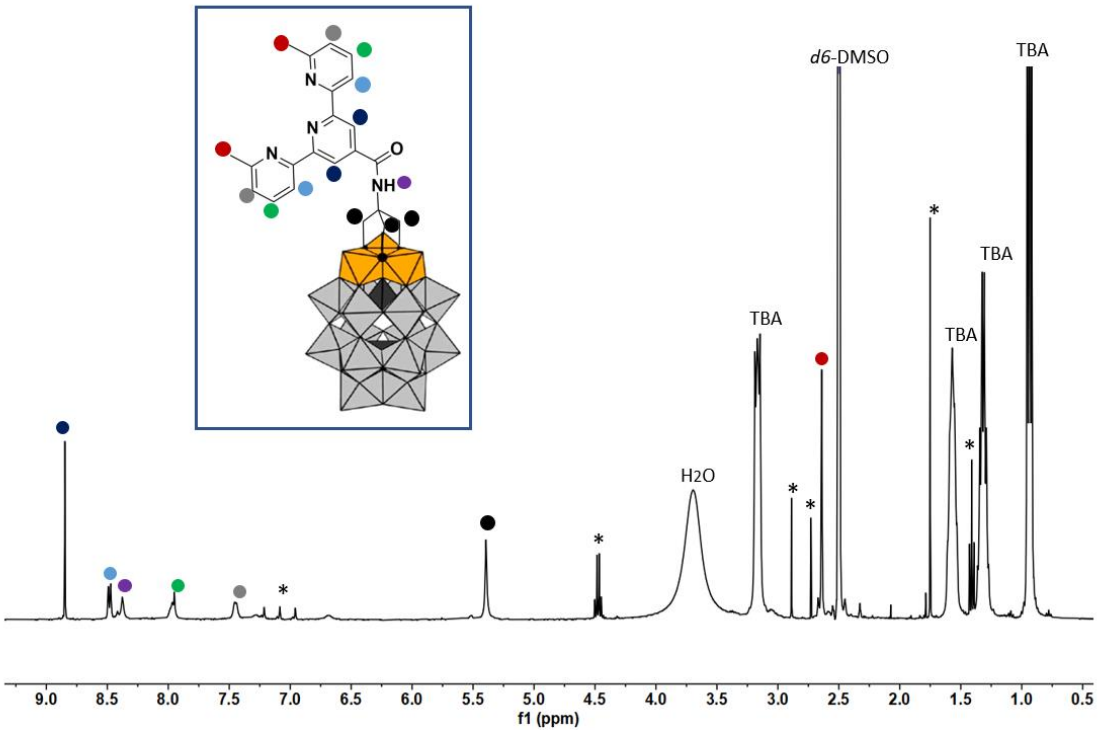

Fig. S18. ^{1}H NMR spectrum of hybrid **H4^{cov} (H1^{cov} + ZnCl$_2$)** in DMSO-*d*$_6$ at 400 MHz.

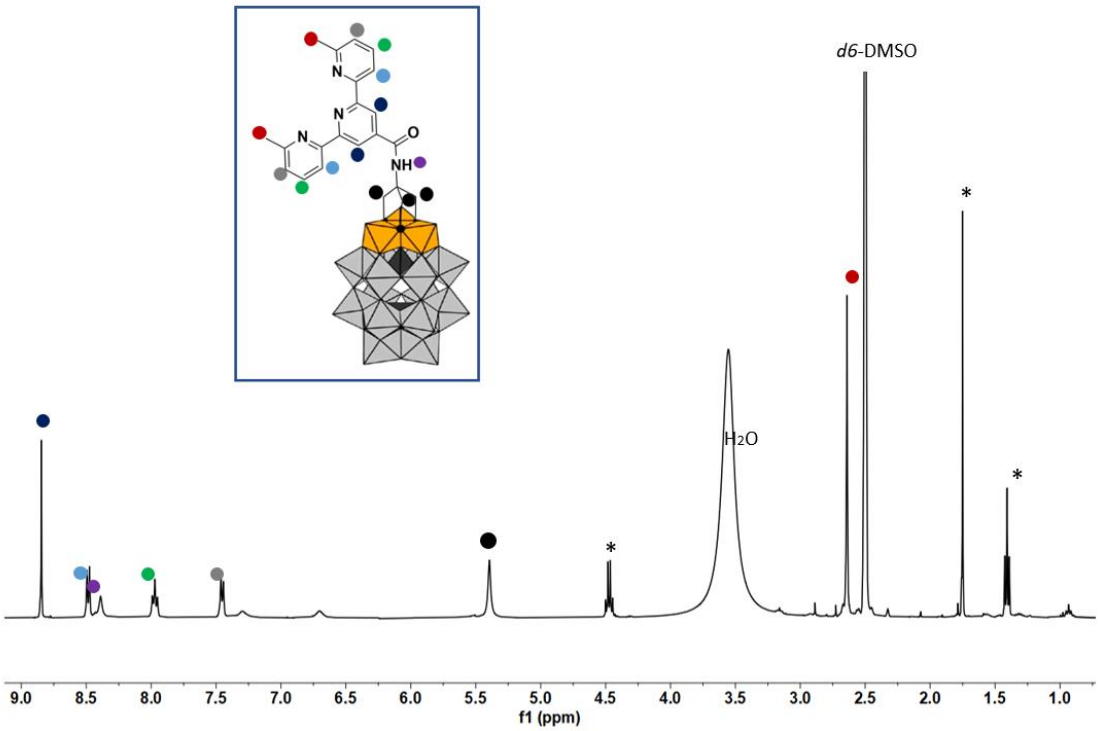

Fig. S19. ^{1}H NMR spectrum of hybrid **H5^{cov} (H1^{cov} + Zn(ClO$_4$)$_2$)** in DMSO-*d*$_6$ at 400 MHz.

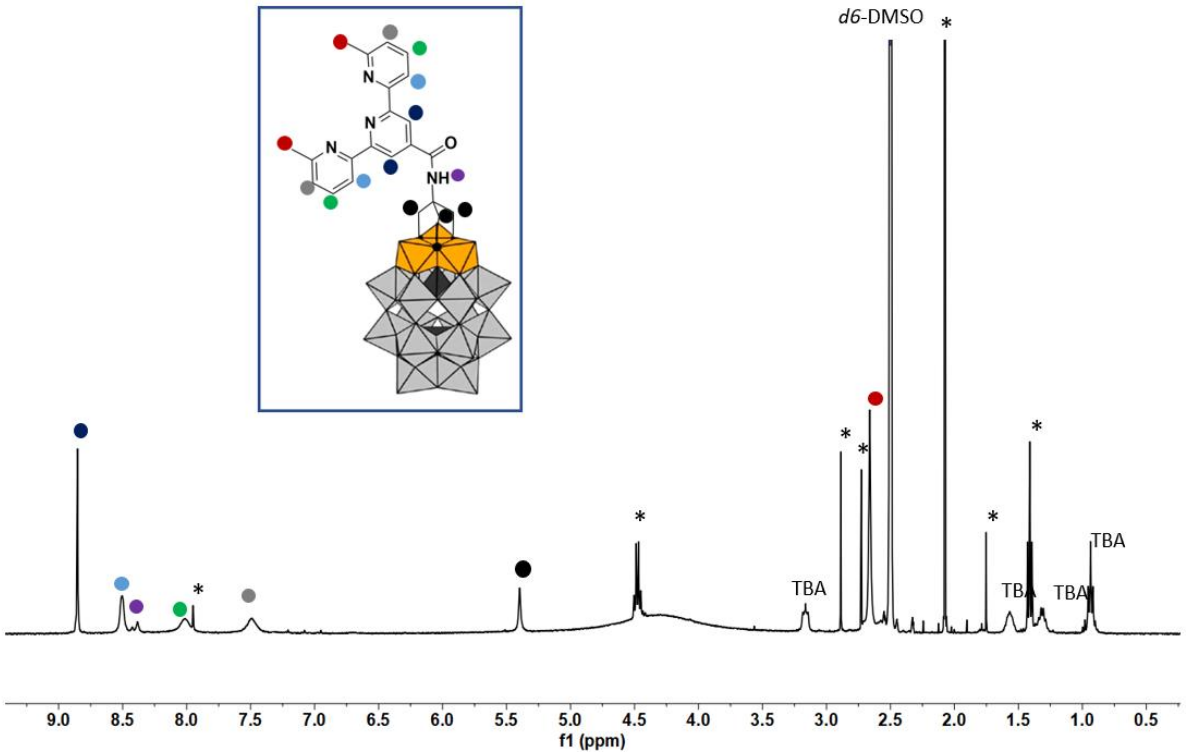

Fig. S20. ^{1}H NMR spectrum of hybrid **H6^{cov} (POM + L^{tpy} + ZnCl$_2$)** in DMSO-*d*$_6$ at 400 MHz.

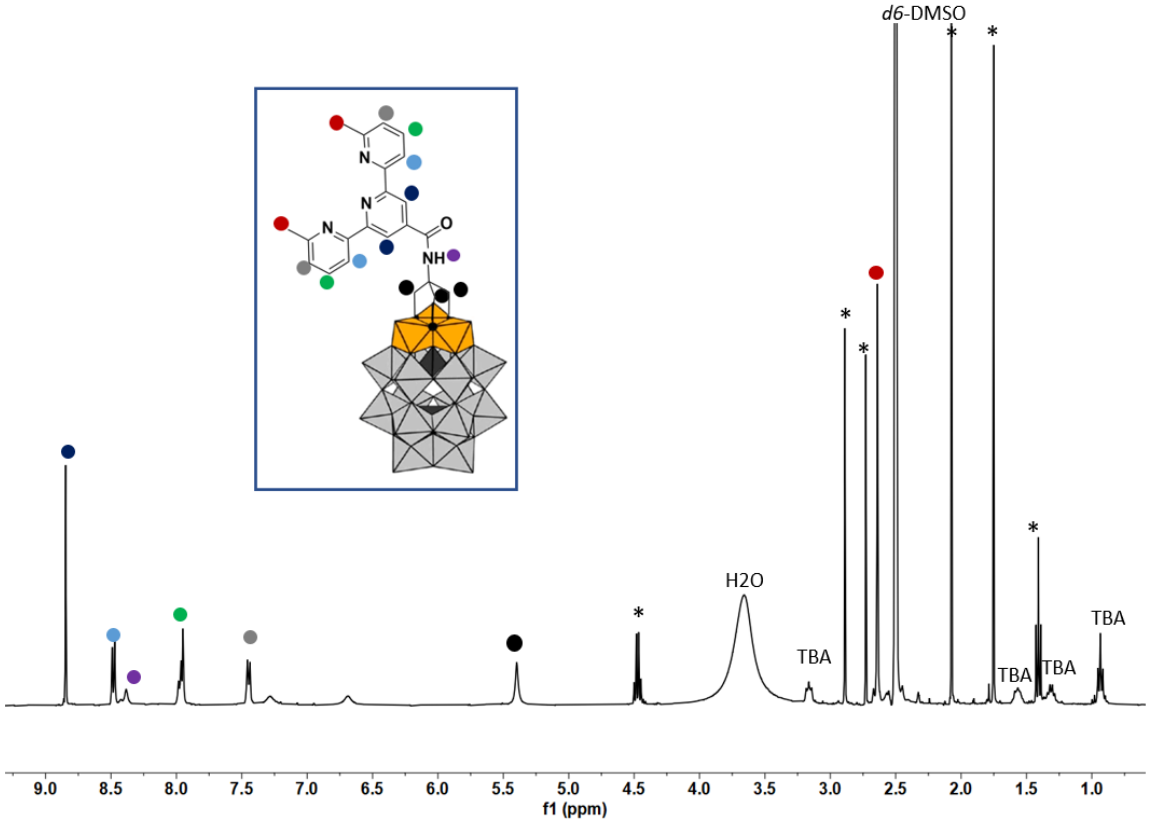

Fig. S21. ^{1}H NMR spectrum of hybrid **H7^{cov} (POM + L^{tpy} + Zn(ClO$_4$)$_2$)** in DMSO-*d*$_6$ at 400 MHz.

5. Comparison of ^{1}H NMR spectra of compounds

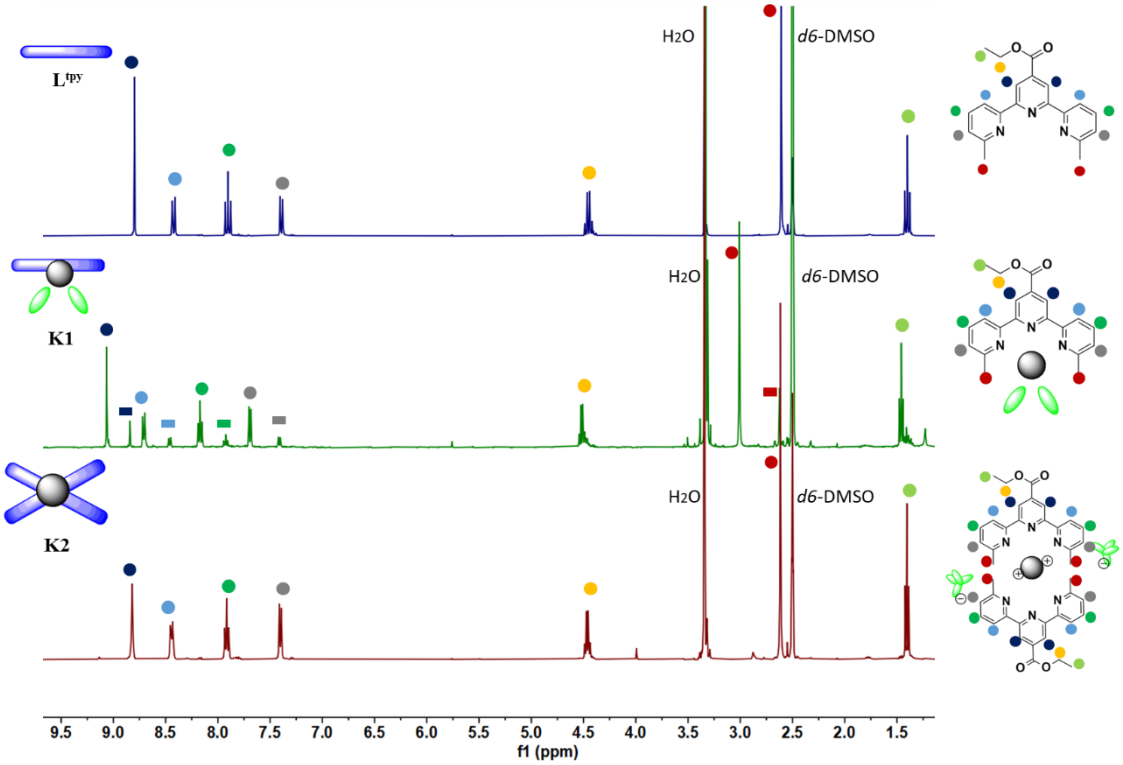

Fig. S22. Comparison of ^{1}H NMR spectra of ligand $\mathbf{L^{tpy}}$ (blue), complex **K1** (green) and complex **K2** (red) in DMSO-d_6 at 400 MHz.

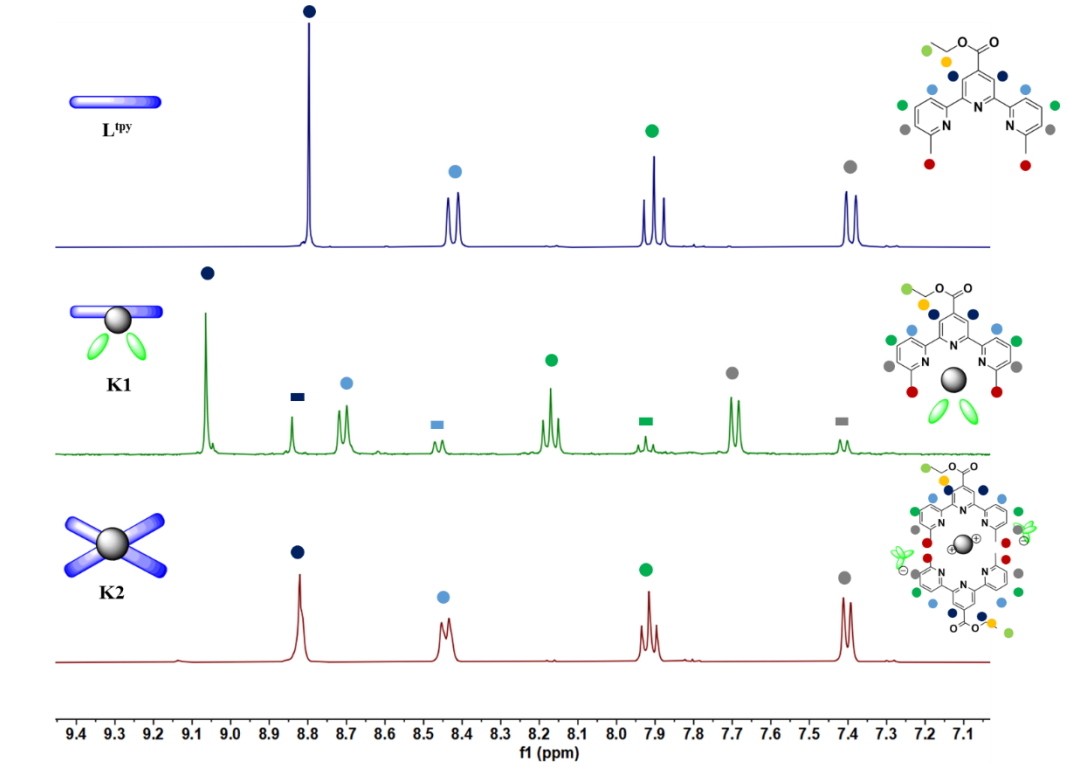

Fig. S23. Comparison of ^{1}H NMR spectra of ligand **L^{tpy}** (blue), complex **K1** (green) and complex **K2** (red) in DMSO-d_6 at 400 MHz (aromatic region).

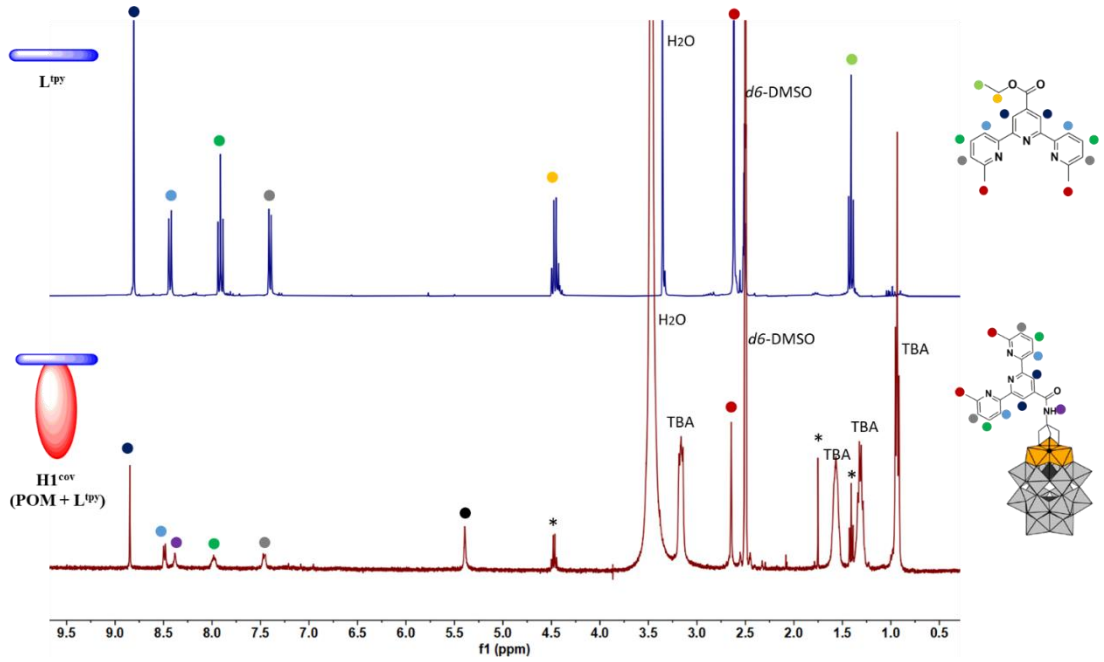

Fig. S24. Comparison of ^{1}H NMR spectra of ligand **L^{tpy}** (blue) and hybrid **H1^{cov} (POM + L^{tpy})** (red) in DMSO-d_6 at 400 MHz.

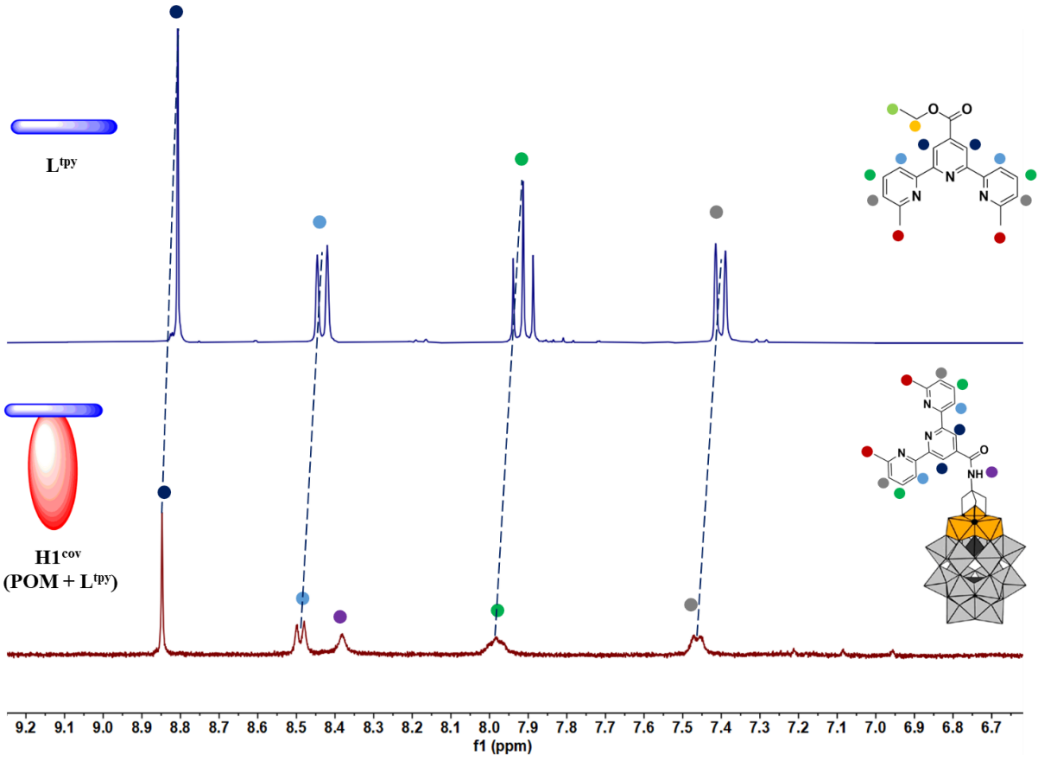

Fig. S25. Comparison of ^{1}H NMR spectra of ligand **L^{tpy}** (blue) and hybrid **H1^{cov} (POM + L^{tpy})** (red) in DMSO-d_6 at 400 MHz (aromatic region).

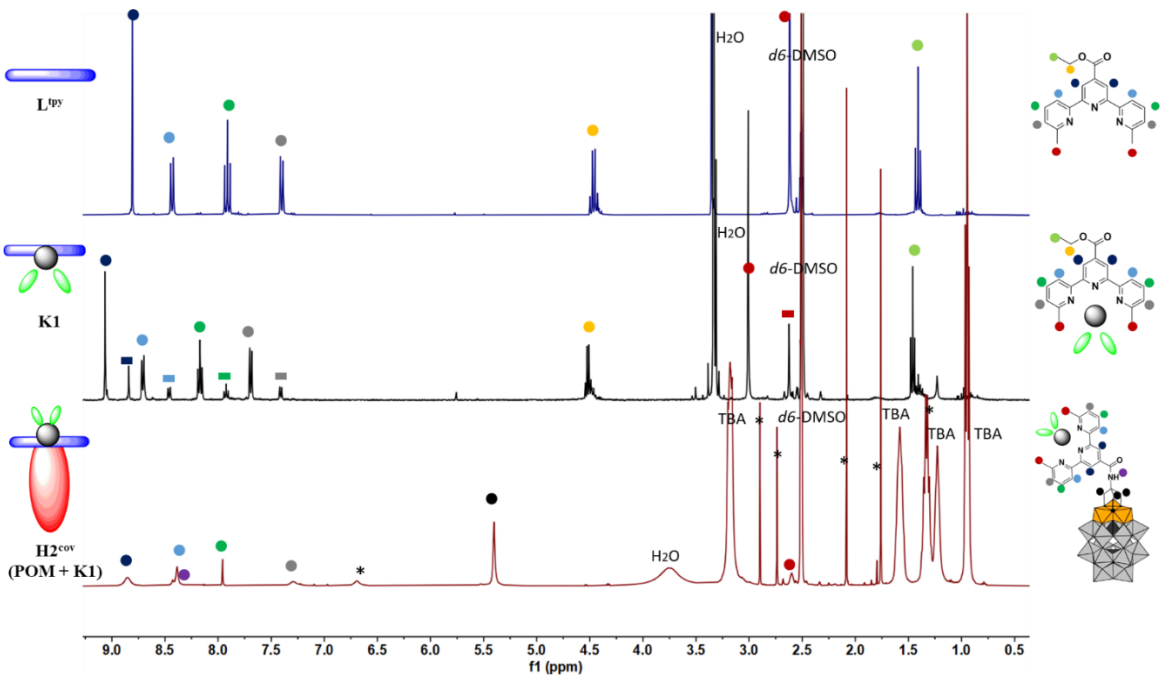

Fig. S26. Comparison of ^{1}H NMR spectra of ligand **L^{tpy}** (blue), complex **K1** (black) and hybrid **H2^{cov} (POM + K1)** (red) in DMSO-d_6 at 400 MHz.

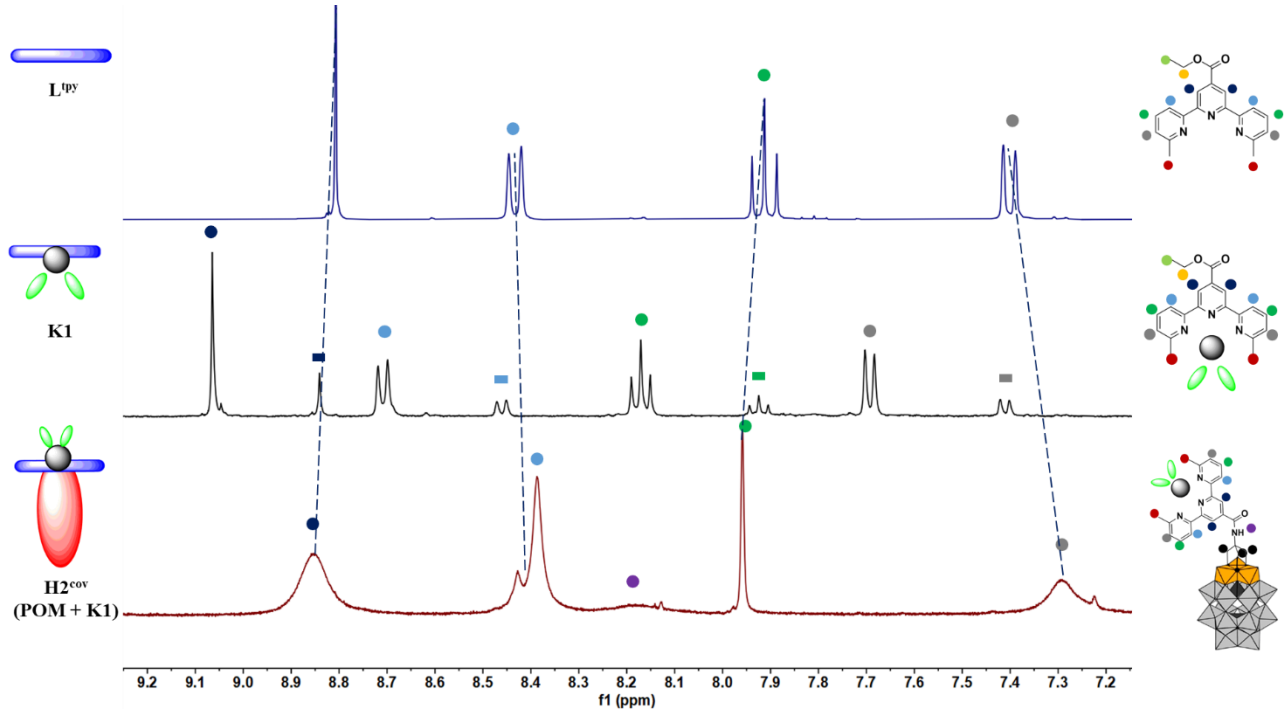

Fig. S27. Comparison of ^{1}H NMR spectra of ligand **L^{tpy}** (blue), complex **K1** (black) and hybrid **H2^{cov} (POM + K1)** (red) in DMSO-d_6 at 400 MHz (aromatic region).

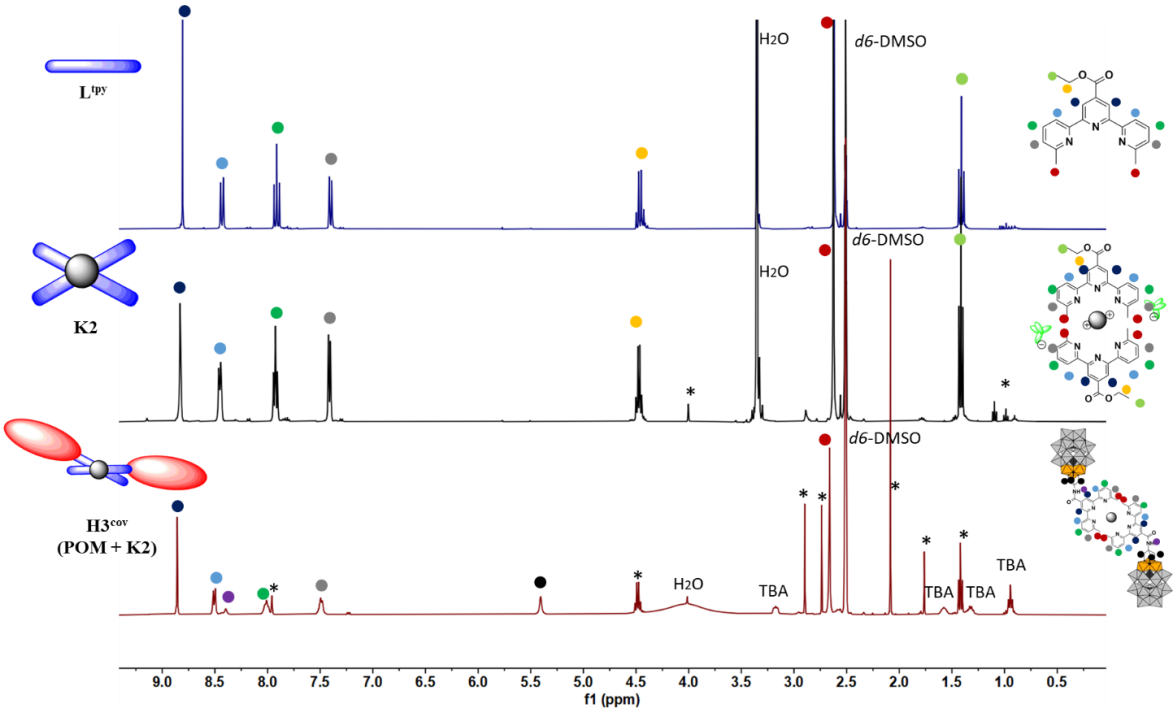

Fig. S28. Comparison of ^{1}H NMR spectra of ligand **L^{tpy}** (blue), complex **K2** (black) and hybrid **H3^{cov} (POM + K2)** (red) in DMSO-d_6 at 400 MHz.

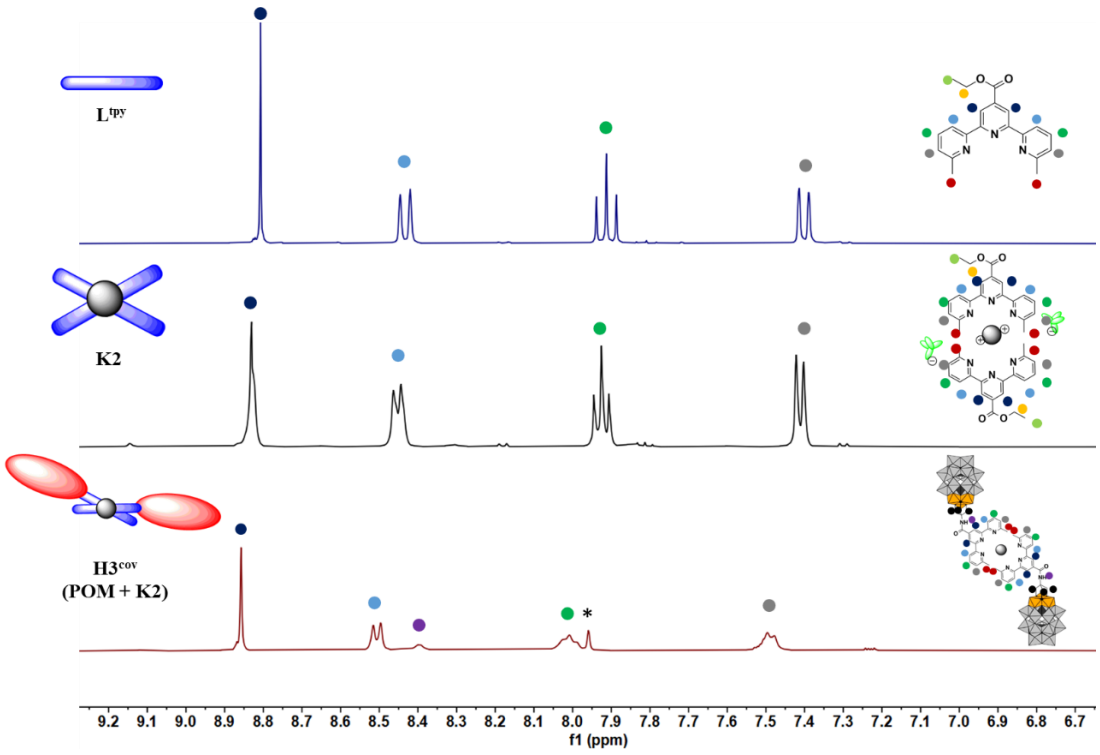

Fig. S29. Comparison of ^{1}H NMR spectra of ligand **L^{tpy}** (blue), complex **K2** (black) and hybrid **H3^{cov} (POM + K2)** (red) in DMSO-*d*$_6$ at 400 MHz (aromatic region).

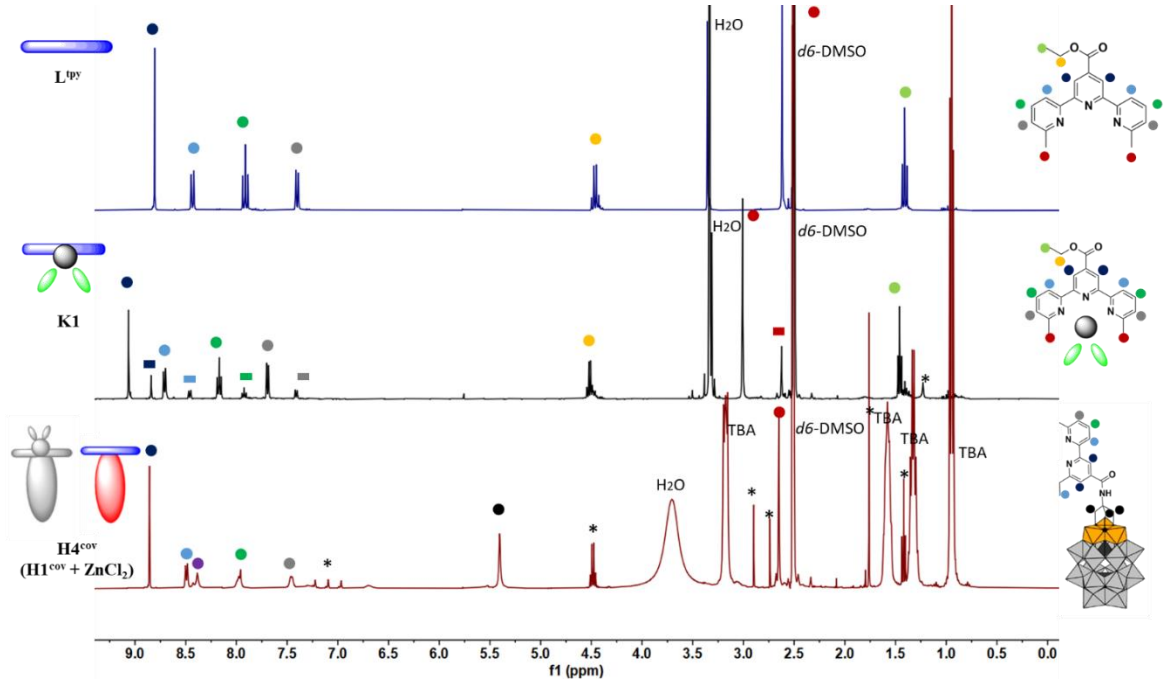

Fig. S30. Comparison of ^{1}H NMR spectra of ligand **L^{tpy}** (blue), complex **K1** (black) and hybrid **H4^{cov} (H1^{cov} + ZnCl$_2$)** (red) in DMSO-*d*$_6$ at 400 MHz.

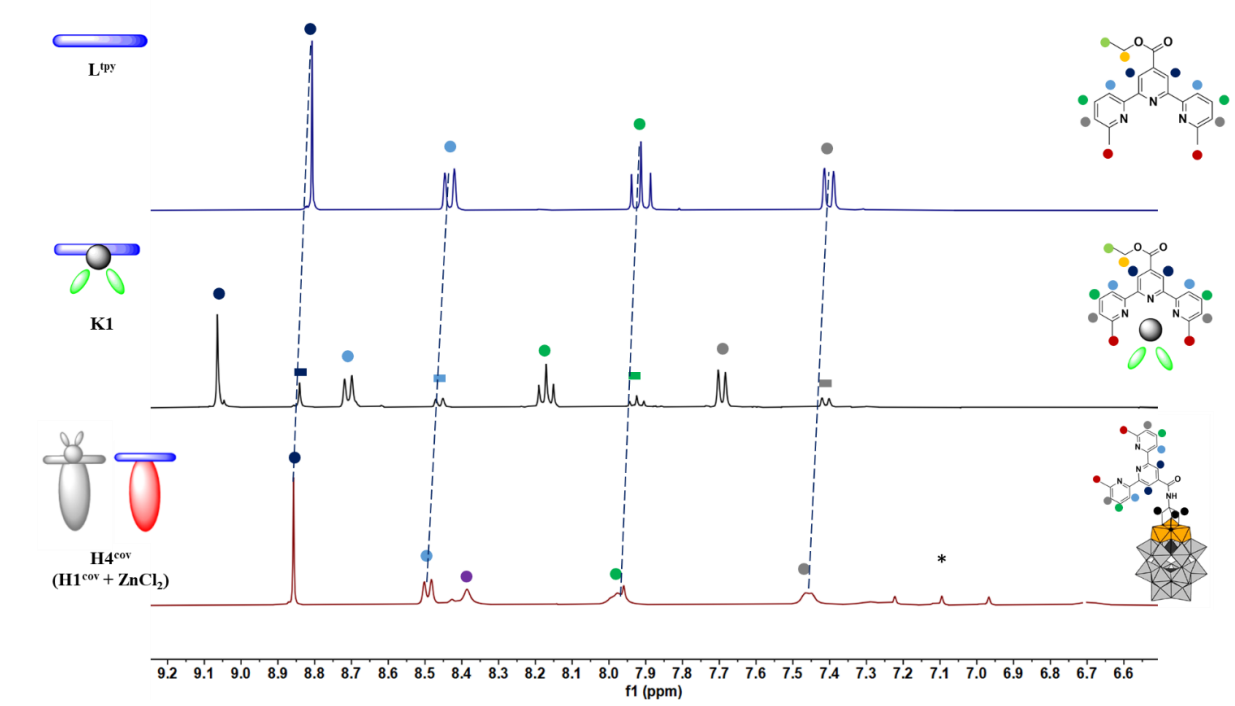

Fig. S31. Comparison of ^{1}H NMR spectra of ligand **L^{tpy}** (blue), complex **K1** (black) and hybrid **H4^{cov} (H1^{cov} + ZnCl$_2$)** (red) in DMSO-*d*$_6$ at 400 MHz (aromatic region).

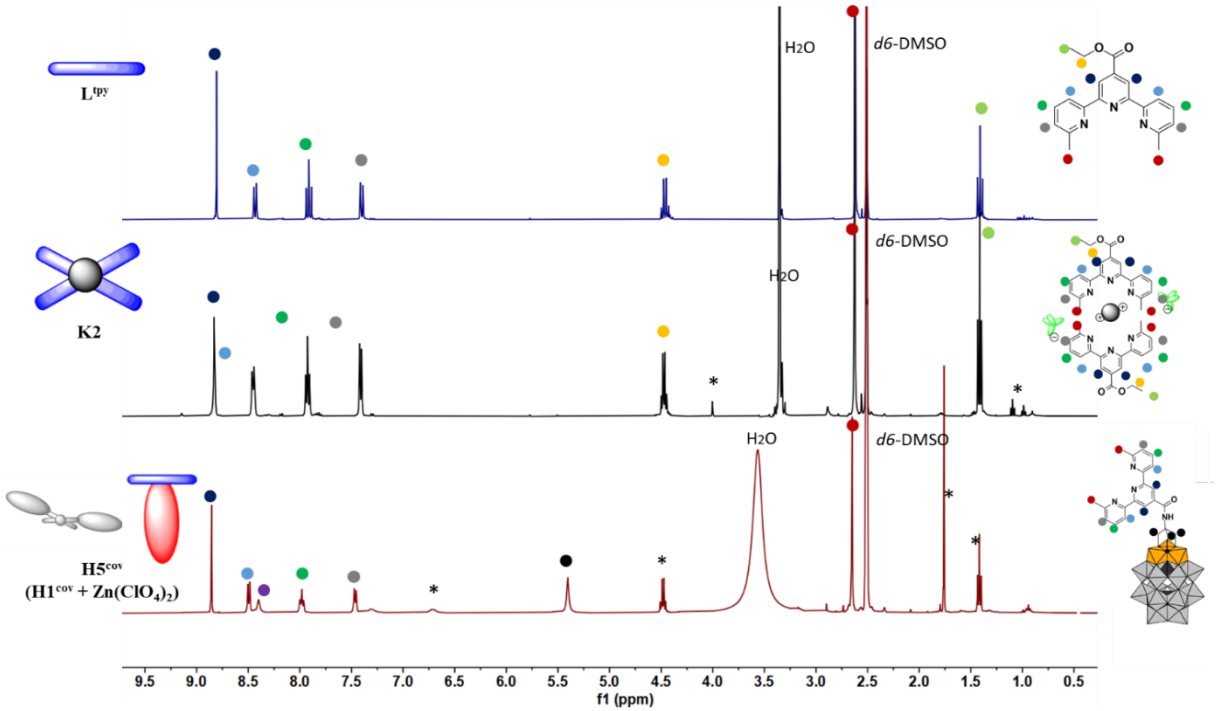

Fig. S32. Comparison of ^{1}H NMR spectra of ligand **L^{tpy}** (blue), complex **K2** (black) and hybrid **H5^{cov} (H1^{cov} + Zn(ClO$_4$)$_2$)** (red) in DMSO-*d*$_6$ at 400 MHz.

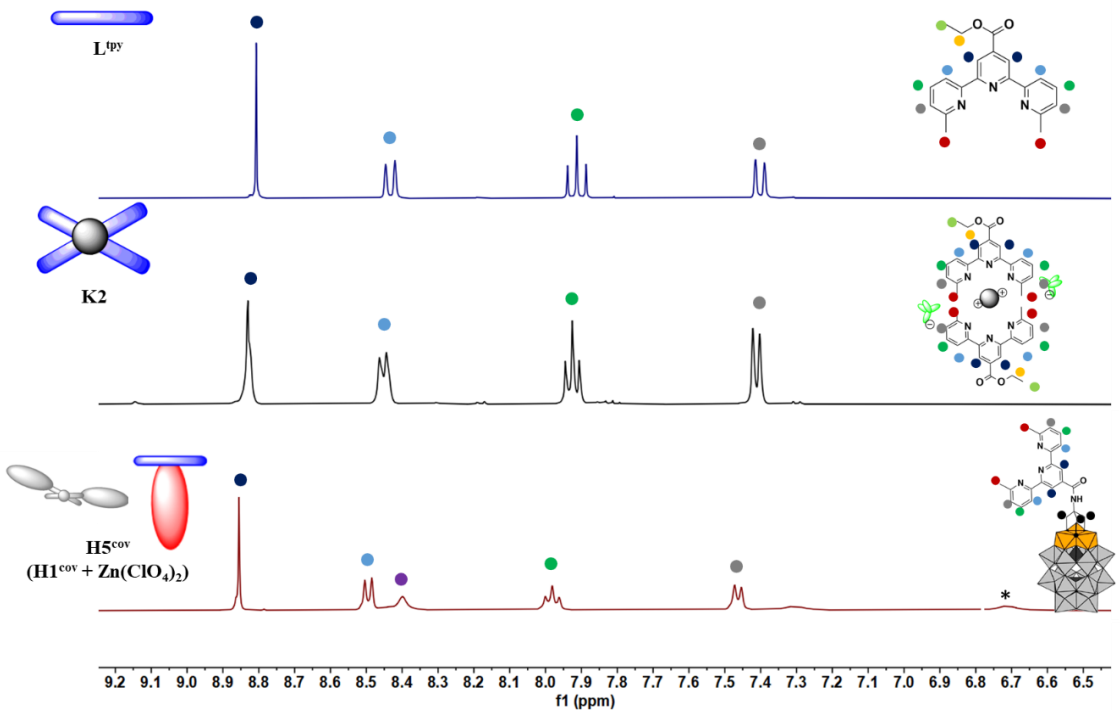

Fig. S33. Comparison of ^{1}H NMR spectra of ligand **L^{tpy}** (blue), complex **K2** (black) and hybrid **H5^{cov} (H1^{cov} + Zn(ClO$_4$)$_2$)** (red) in DMSO-*d*$_6$ at 400 MHz (aromatic region).

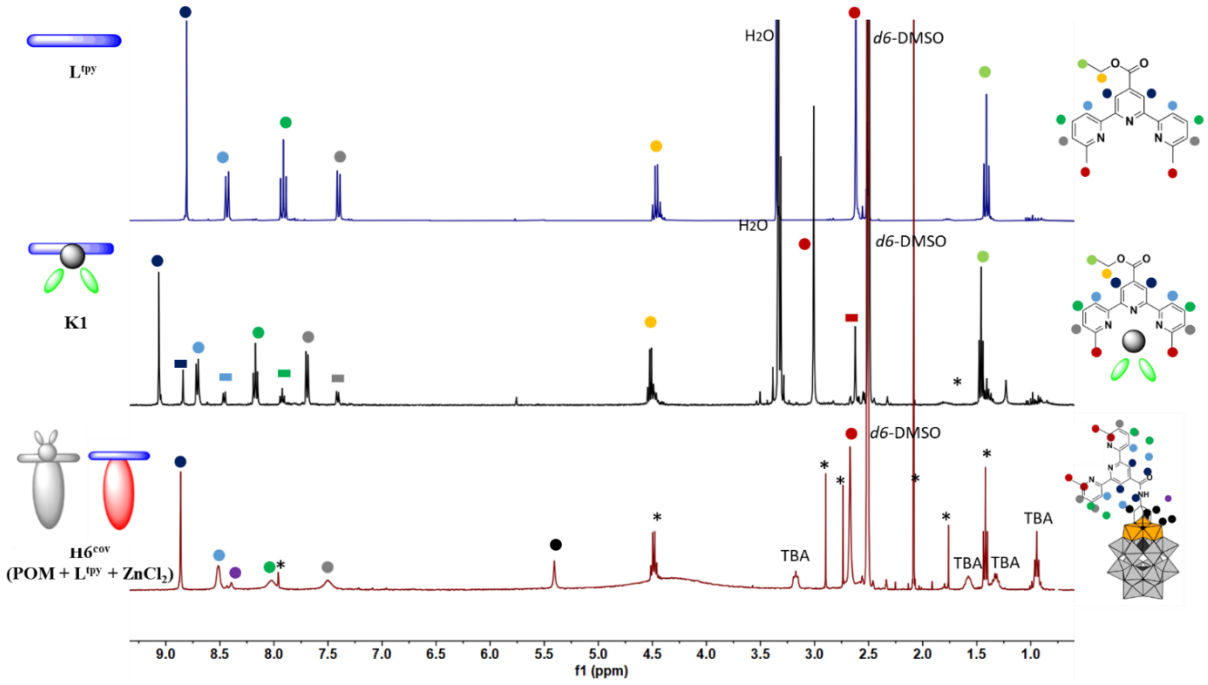

Fig. S34. Comparison of ^{1}H NMR spectra of ligand **L^{tpy}** (blue), complex **K1** (black) and hybrid **H6^{cov} (POM + L^{tpy} + ZnCl$_2$)** (red) in DMSO-*d*$_6$ at 400 MHz.

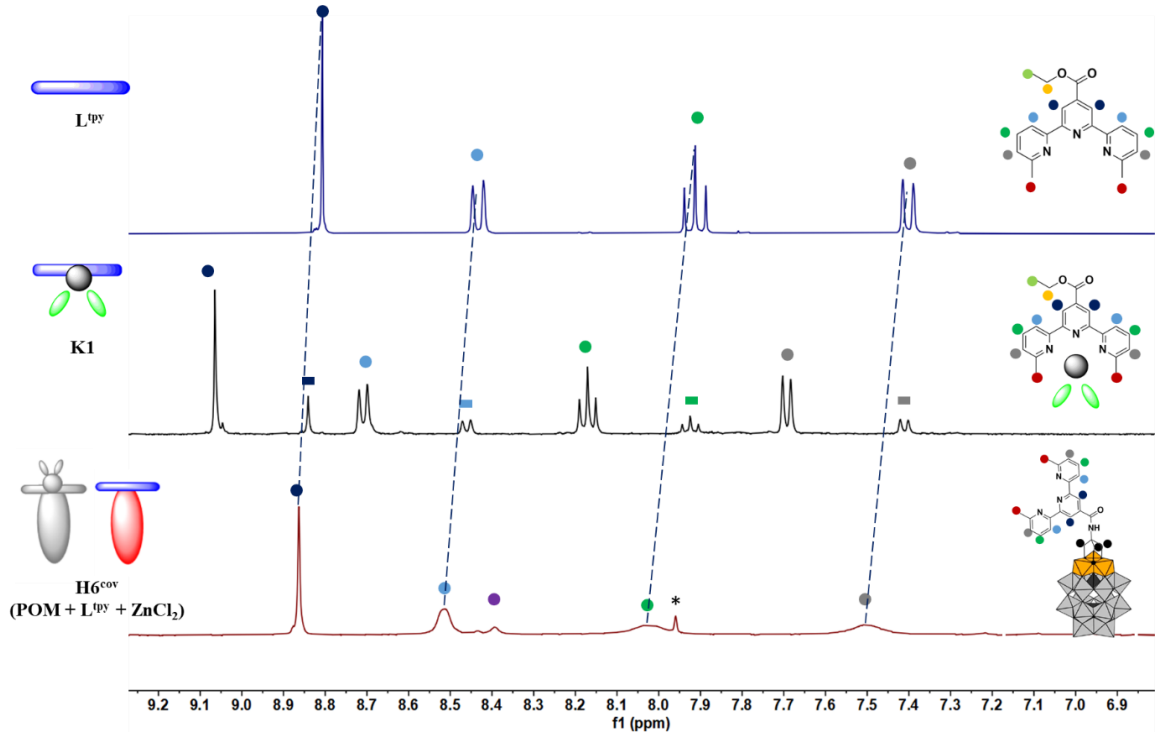

Fig. S35. Comparison of ^{1}H NMR spectra of ligand **L^{tpy}** (blue), complex **K1** (black) and hybrid **H6^{cov} (POM + L^{tpy} + ZnCl$_2$)** (red) in DMSO-*d*$_6$ at 400 MHz (aromatic region).

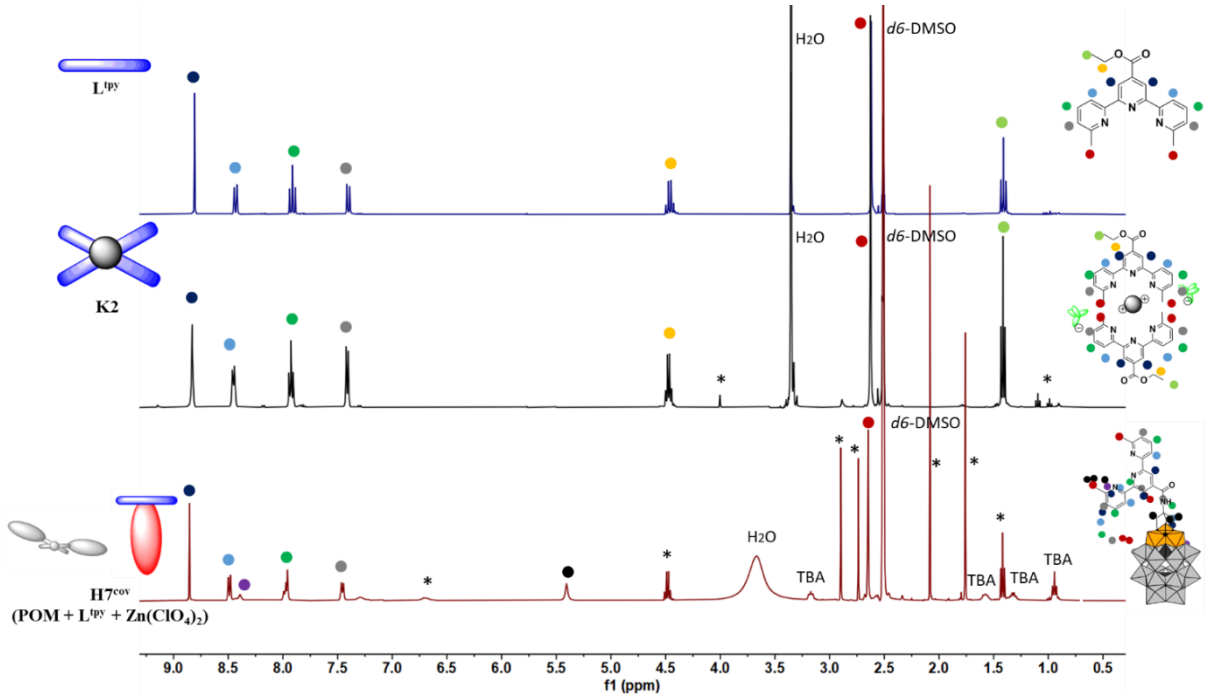

Fig. S36. Comparison of ^{1}H NMR spectra of ligand **L^{tpy}** (blue), complex **K2** (black) and hybrid **H7^{cov} (POM + L^{tpy} + Zn(ClO$_4$)$_2$)** (red) in DMSO-*d*$_6$ at 400 MHz.

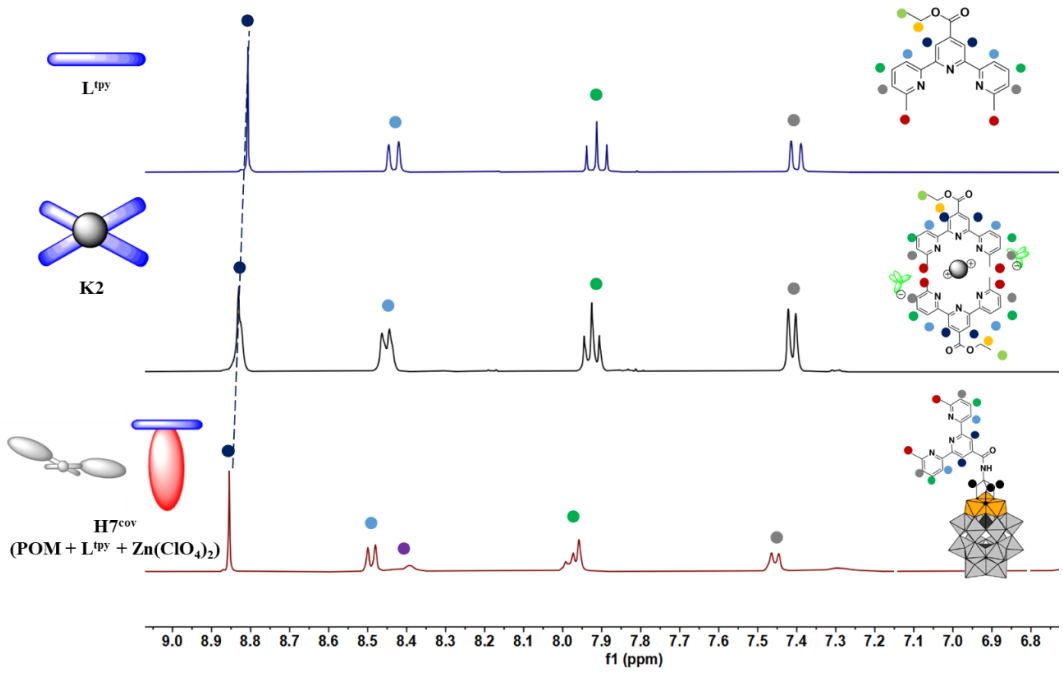

Fig. S37. Comparison of ^{1}H NMR spectra of ligand **L^{tpy}** (blue), complex **K2** (black) and hybrid **H7^{cov} (POM + L^{tpy} + Zn(ClO$_4$)$_2$)** (red) in DMSO-d_6 at 400 MHz (aromatic region).

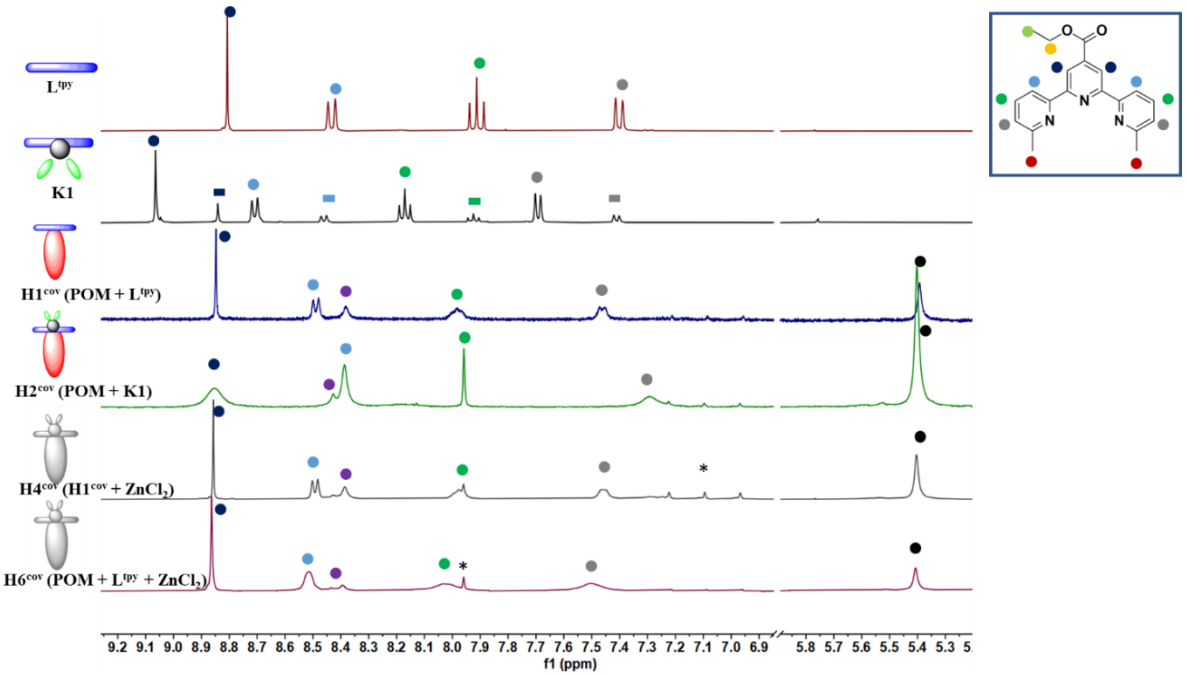

Fig. S38. Comparison of ^{1}H NMR spectra of ligand **L^{tpy}**, complex **K1** and hybrids: **H1^{cov} (POM + L^{tpy}), H2^{cov} (POM + K1), H4^{cov} (H1^{cov} + ZnCl$_2$), H6^{cov} (POM + L^{tpy} + ZnCl$_2$)**, respectively in DMSO-d_6 at 400 MHz.

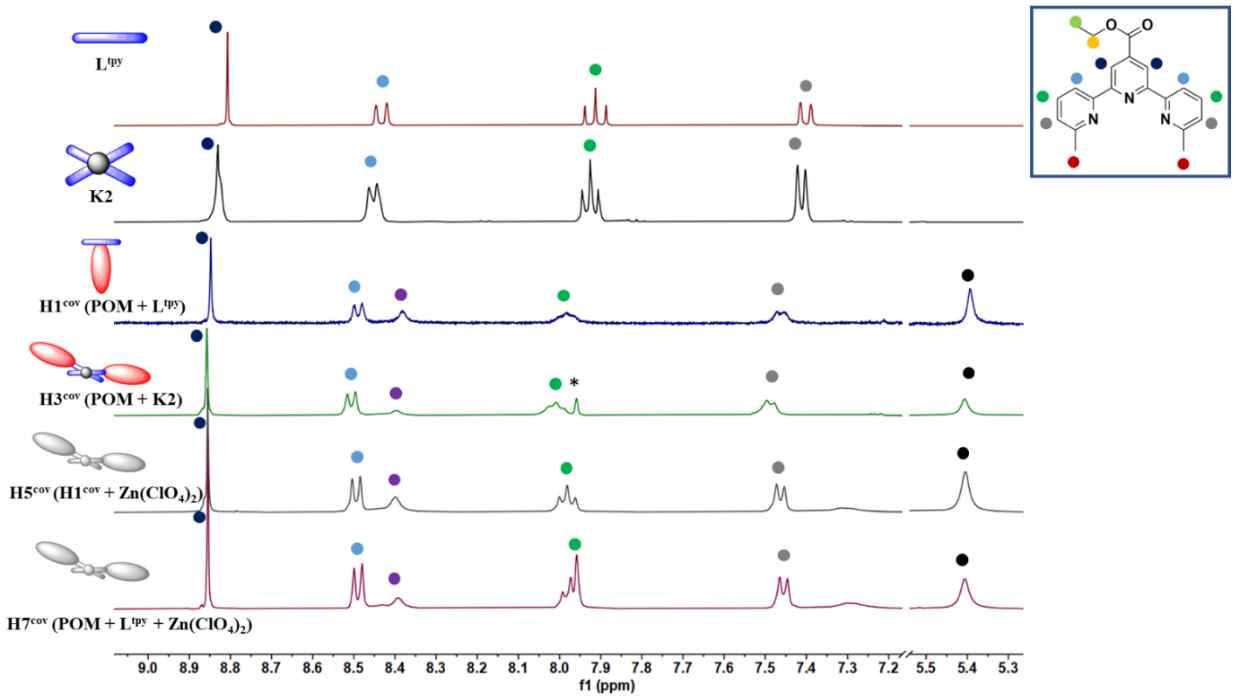

Fig. S39. Comparison of ^{1}H NMR spectra of ligand **L^{tpy}**, complex **K1** and hybrids: **H1^{cov} (POM + L^{tpy}), H3^{cov} (POM + K2), H5^{cov} (H1^{cov} + Zn(ClO$_4$)$_2$), H7^{cov} (POM + L^{tpy} + Zn(ClO$_4$)$_2$)**, respectively in DMSO-*d*$_6$ at 400 MHz.

6. ^{31}P NMR spectra of hybrids

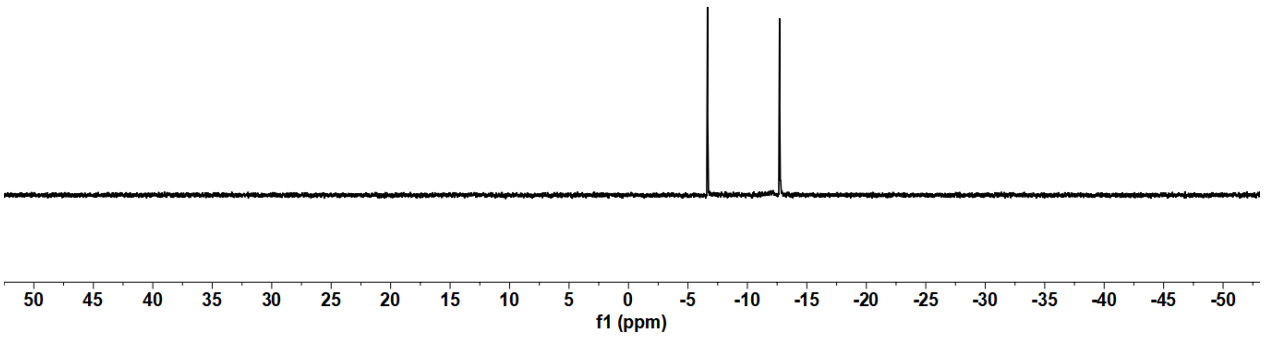

Fig. S40. ^{31}P NMR spectrum of hybrid **H1^{cov} (POM + L^{tpy})** in DMSO-*d*$_6$ at 400 MHz.

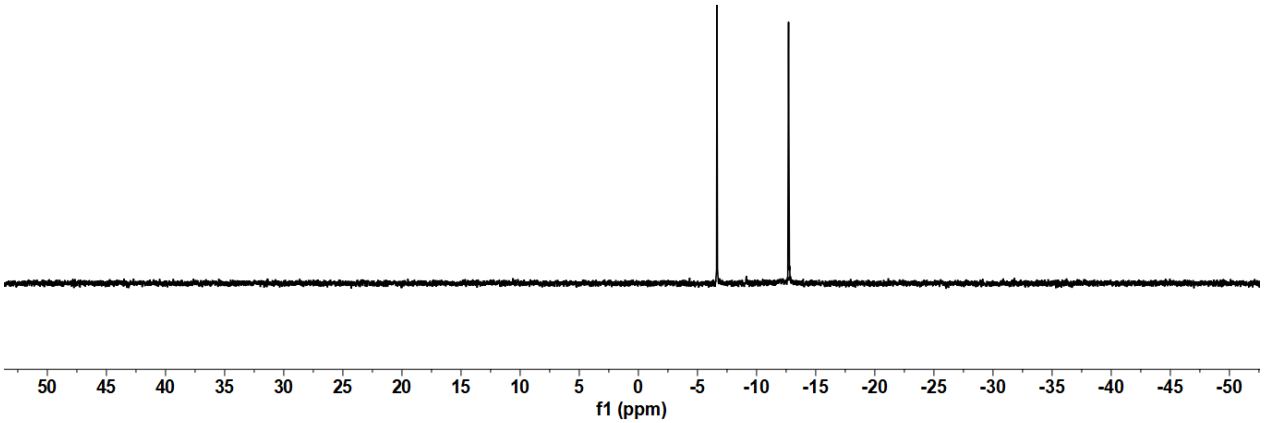

Fig. S41. ^{31}P NMR spectrum of hybrid **H2^{cov} (POM + K1)** in DMSO-d_6 at 400 MHz.

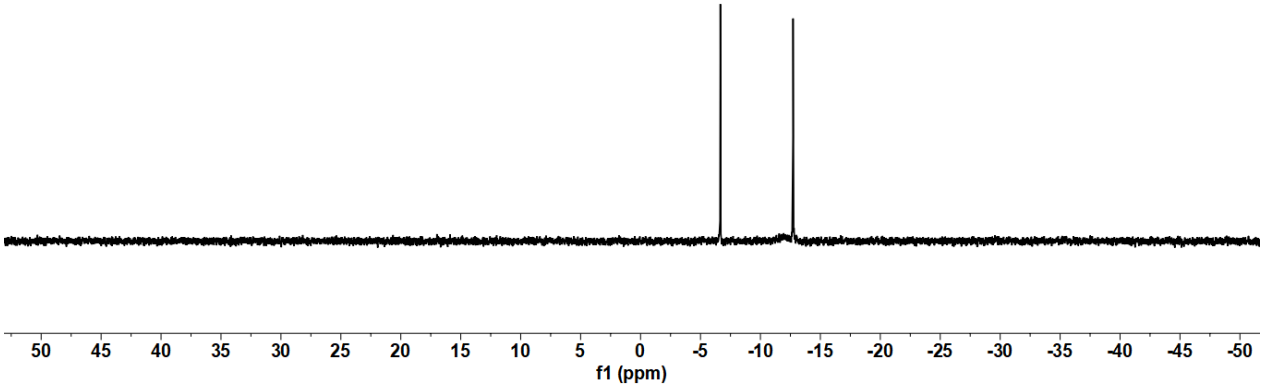

Fig. S42. ^{31}P NMR spectrum of hybrid **H3^{cov} (POM + K2)** in DMSO-d_6 at 400 MHz.

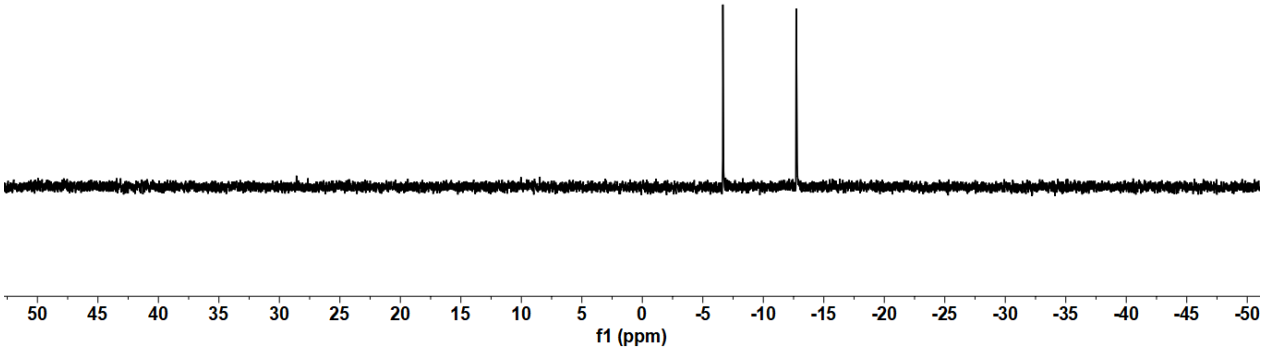

Fig. S43. ^{31}P NMR spectrum of hybrid **H4^{cov} (H1^{cov} + ZnCl$_2$)** in DMSO-d_6 at 400 MHz.

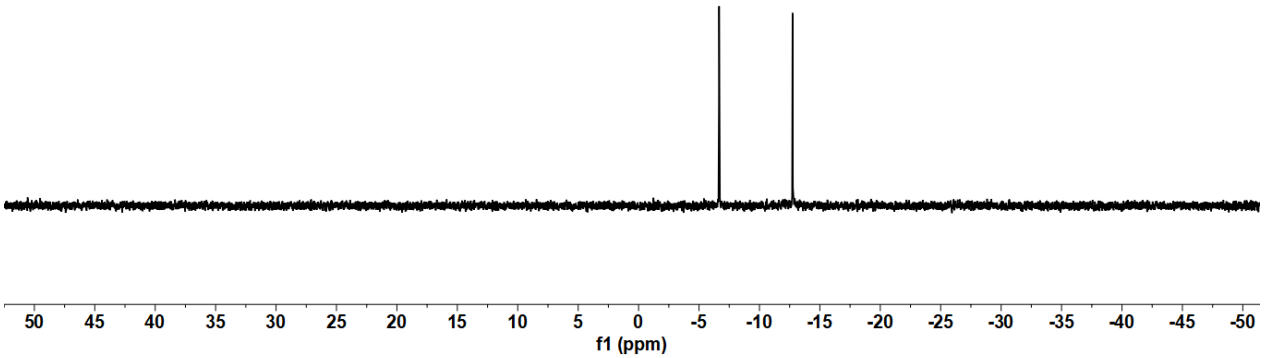

Fig. S44. ^{31}P NMR spectrum of hybrid **H5^{cov} (H1^{cov} + Zn(ClO$_4$)$_2$)** in DMSO-d_6 at 400 MHz.

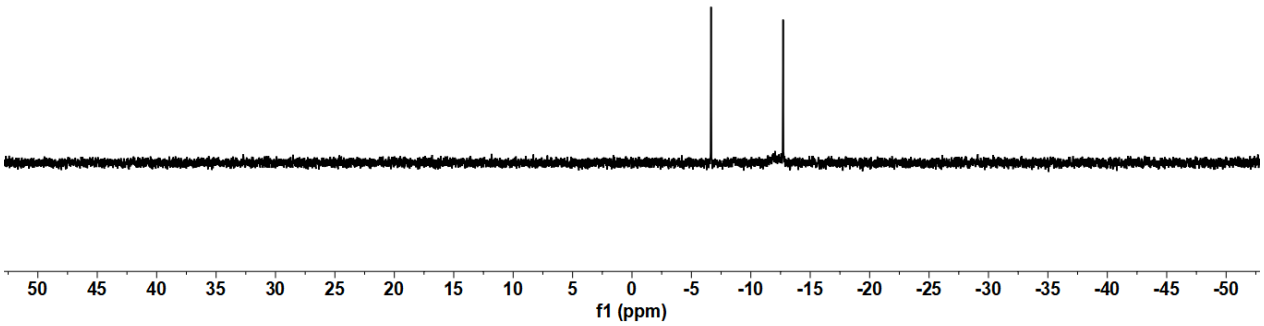

Fig. S45. ^{31}P NMR spectrum of hybrid **H6^{cov} (POM + L^{tpy} + ZnCl$_2$)** in DMSO-d_6 at 400 MHz.

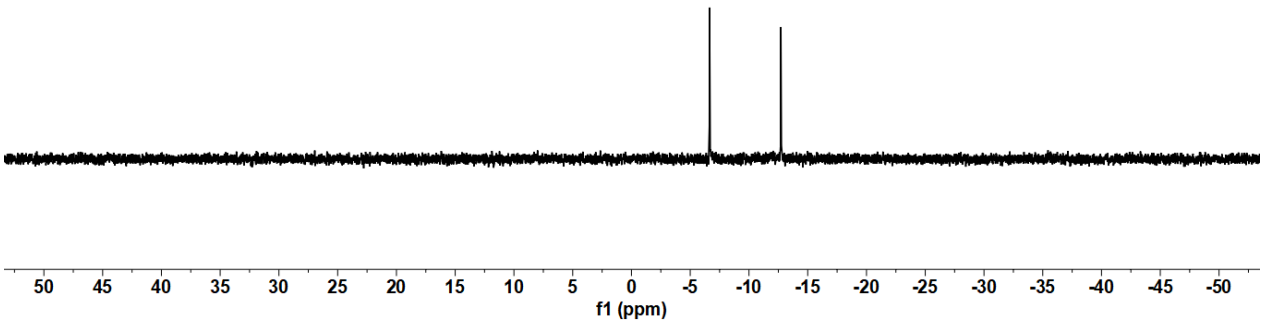

Fig. S46. ^{31}P NMR spectrum of hybrid **H7^{cov} (POM + L^{tpy} + Zn(ClO$_4$)$_2$)** in DMSO-d_6 at 400 MHz.

7. Comparison of ^{31}P NMR spectra of hybrids

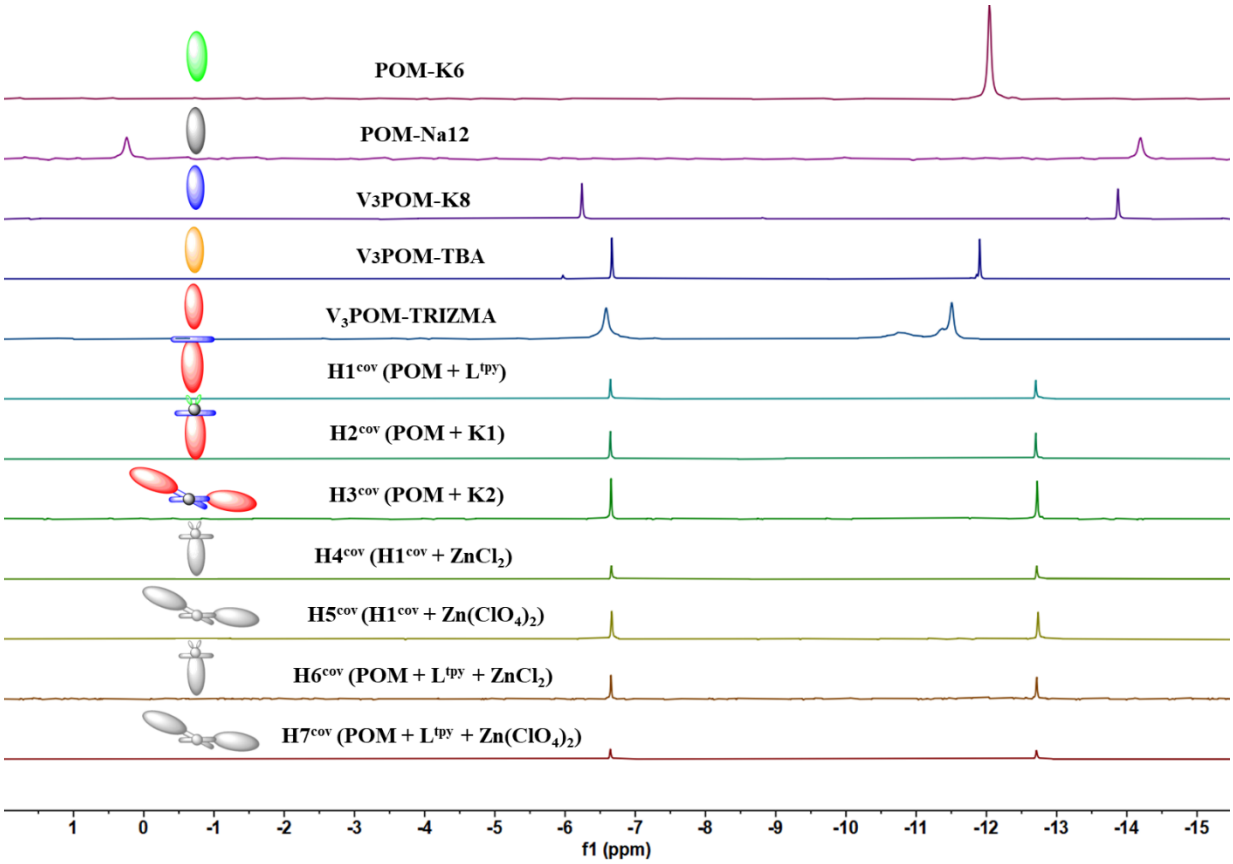

Fig. S47. Comparison of ^{31}P NMR spectra of hybrids: **POM-K6, POM-Na12, V_3POM-K8, V_3POM-TBA, V_3POM-TRIZMA, H1^{cov} (POM + L^{tpy}), H2^{cov} (POM + K1), H3^{cov} (POM + K2), H4^{cov} (H1^{cov} + $ZnCl_2$), H5^{cov} (H1^{cov} + $Zn(ClO_4)_2$), H6^{cov} (POM + L^{tpy} + $ZnCl_2$), H7^{cov} (POM + L^{tpy} + $Zn(ClO_4)_2$)**, respectively in DMSO-d_6 at 400 MHz.

8. Biological measurements

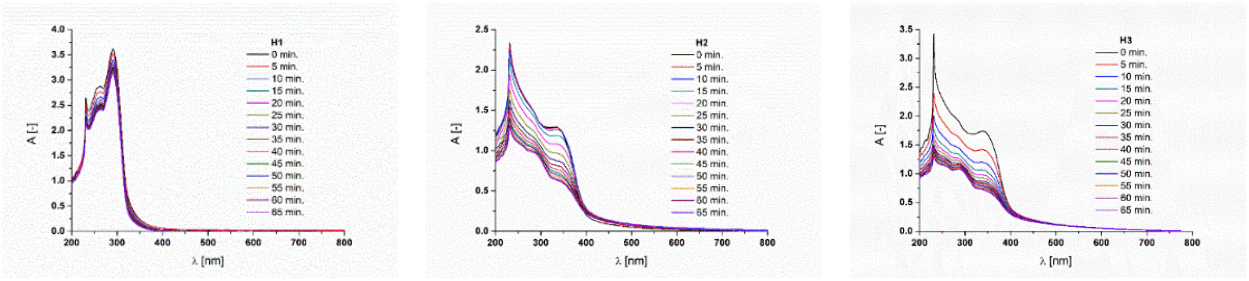

Fig. S48. Time-dependent equilibration of **H1^{ion}** and **H2^{ion}** and **H3^{ion}** in Tris Buffer with 1% DMSO content.

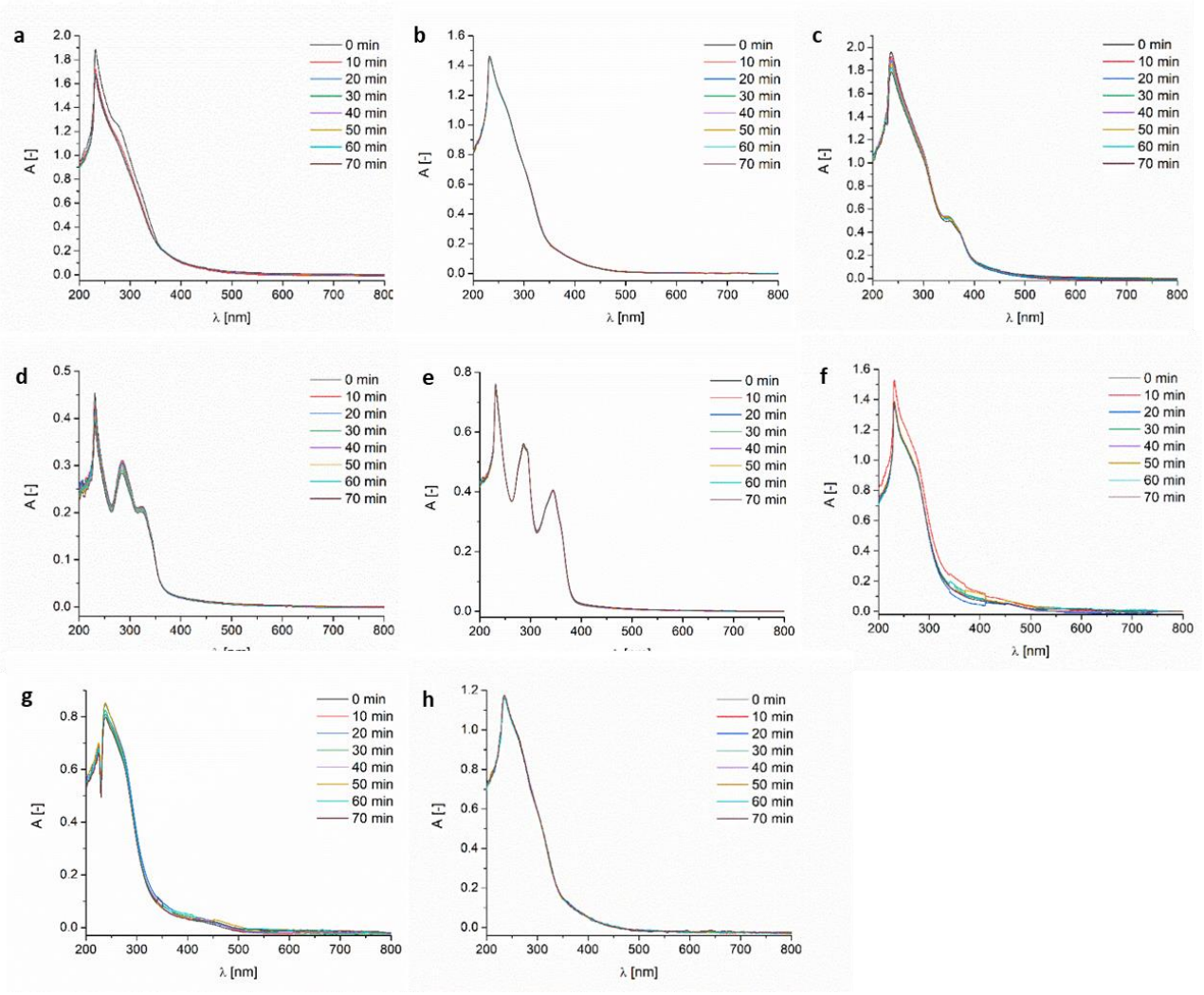

Fig. S49. Time-dependent equilibration of (a) **H1^{cov}**, (b) **H2^{cov}**, (c) **H3^{cov}**, (d) **L**, (e) **K2**, (f) **V$_3$P-K8**, (g) **V$_3$P-TBA** and (h) **V$_3$P+trizma** in Tris Buffer (5 mM Tris, 50 mM NaCl, pH = 7.4) with 1% DMSO content.

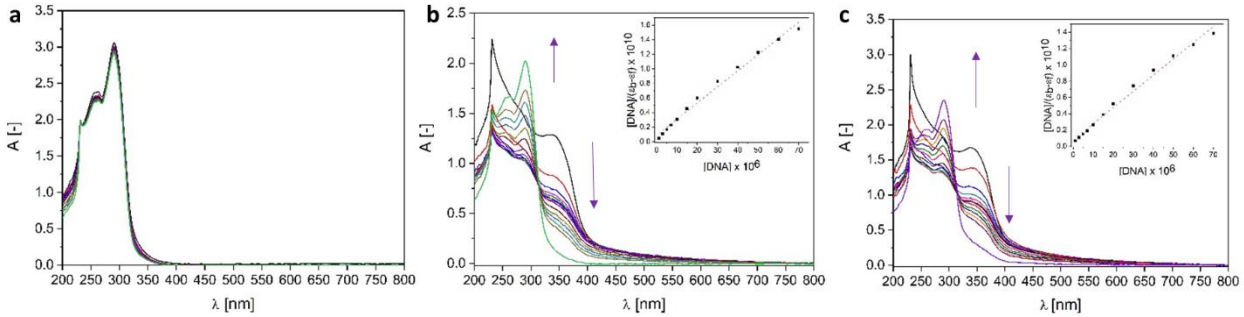

Fig. S50. Titration of (a) **H1^{ion}** and (b/c) **H2^{ion} / H3^{ion}** CD-SECs with aliquots of CT-DNA in (5 mM Tris, 50 mM NaCl, pH = 7.4) with 1% DMSO content. Arrows show changes upon increasing CT-DNA concentration. Insets in **b** and **c**: plot of [DNA]/(ε_a-ε_f) versus [DNA]; ■, experimental data points; solid line, linear fitting of the data.

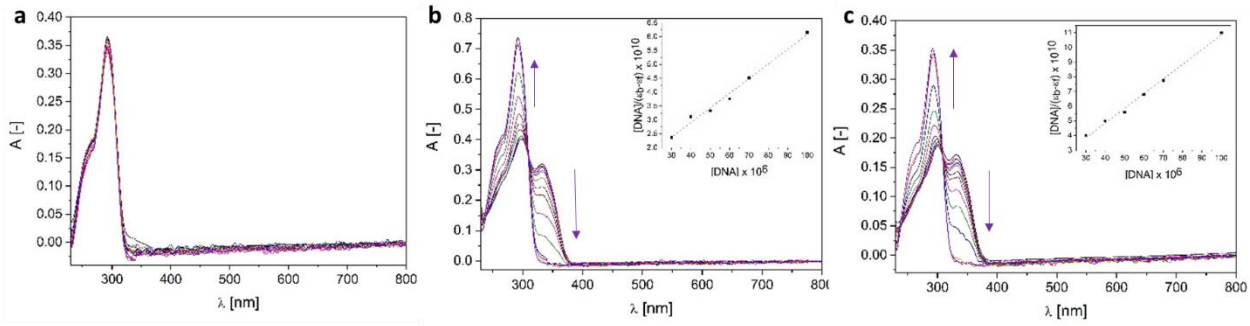

Fig. S51. Titration of (a) **L^{N2O}**, (b) **K1^{ion}** and (c) **K2^{ion}** with aliquots of CT-DNA in (5 mM Tris, 50 mM NaCl, pH = 7.4) with 1% DMSO content. Arrows show changes upon increasing CT-DNA concentration. Insets in **b** and **c**: plot of [DNA]/(ε_a-ε_f) versus [DNA]; ■, experimental data points; solid line, linear fitting of the data.

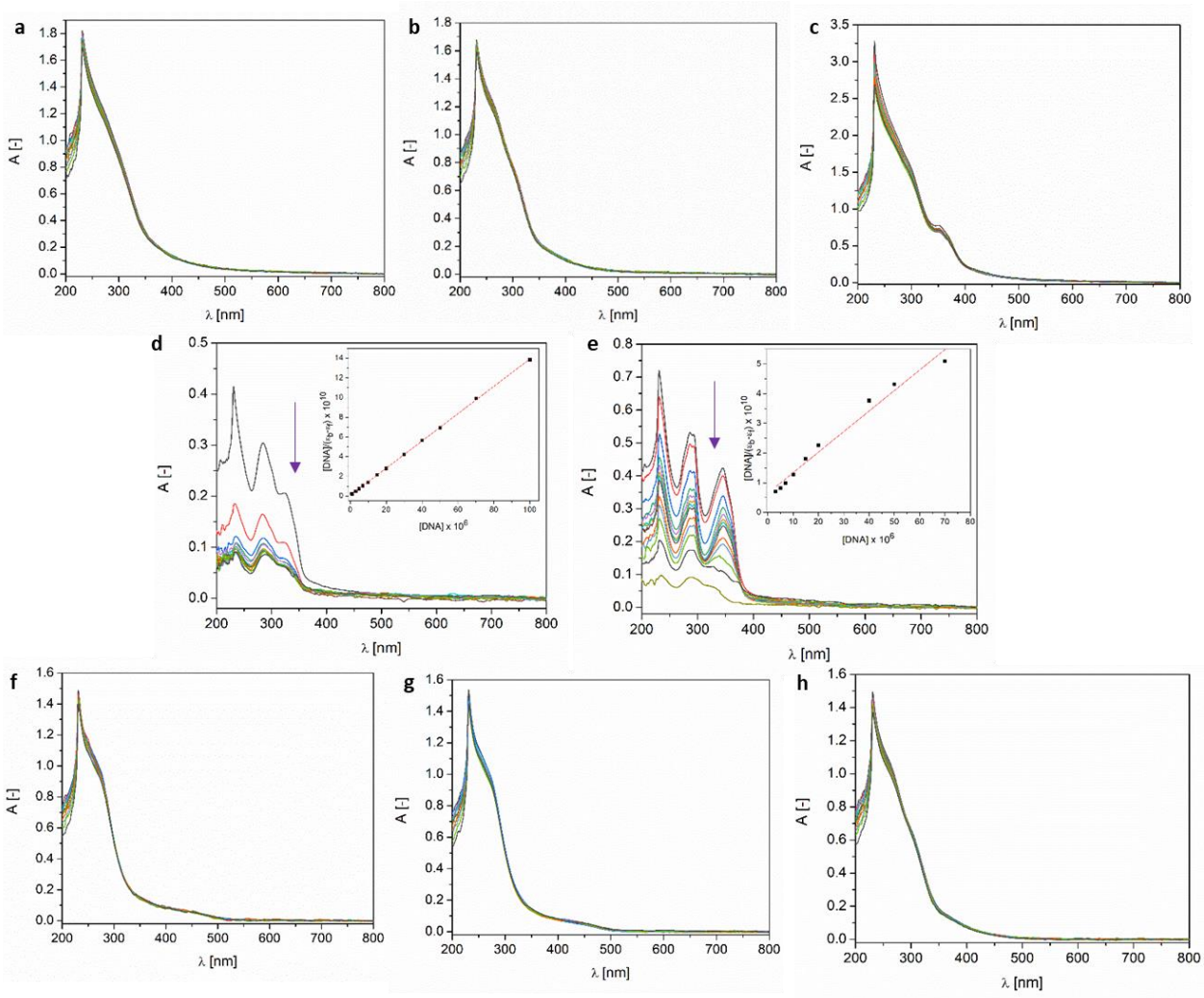

Fig. S52. Titration of (a) **H1^{cov}**, (b) **H2^{cov}**, (c) **H3^{cov}**, (d) **L^{tpy}**, (e) **K2**, (f) **V$_3$P-K8**, (g) **V$_3$P-TBA** and (h) **V$_3$P+trizma** with aliquots of CT-DNA in (5 mM Tris, 50 mM NaCl, pH = 7.4) with 1% DMSO content. Arrows show hypochromic changes upon increasing CT-DNA concentration. Insets in **d** and **e**: plot of [DNA]/(ε_a-ε_f) versus [DNA]; ■, experimental data points; solid line, linear fitting of the data.

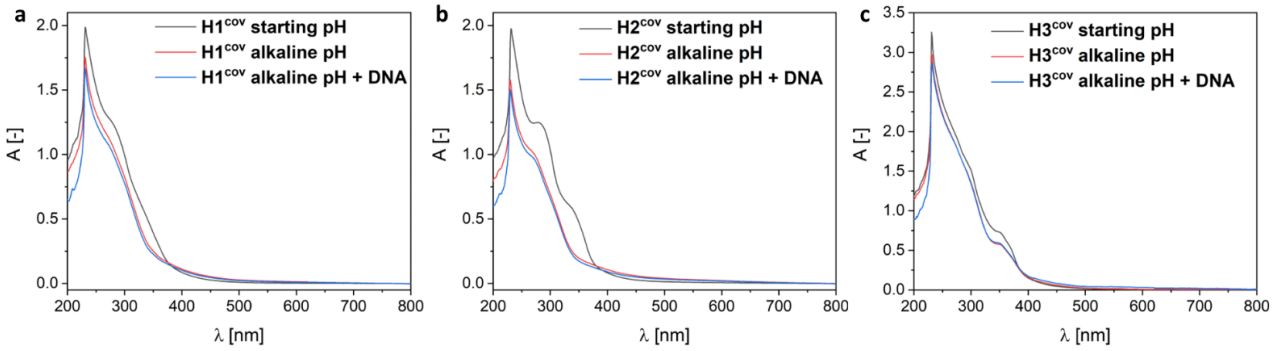

Fig. S53. Investigation on the influence of pH change (to ~8.6) on the stability of (a) **H1^{cov}**, (b) **H2^{cov}** and (c) **H3^{cov}** with subsequent addition of the 100 μM CT-DNA aliquots in miliQ water with 1% DMSO content after 1 h equilibration period.

References

1. G. Ulrich, S. Bedel, C. Picard and P. Tisnès, *Tetrahedron Letters*, 2001, **42**, 6113-6115.